Amplitude analysis of D^{0}→K^{-}π^{+}π^{+}π^{-}

M. Ablikim *et al.* (BESIII Collaboration)

Phys. Rev. D **95**, 072010 — Published 14 April 2017

DOI: 10.1103/PhysRevD.95.072010

Amplitude analysis of $D^0 \to K^-\pi^+\pi^+\pi^-$

M. Ablikim[1], M. N. Achasov[9,e], S. Ahmed[14], X. C. Ai[1], O. Albayrak[5], M. Albrecht[4], D. J. Ambrose[44], A. Amoroso[49A,49C], F. F. An[1], Q. An[46,a], J. Z. Bai[1], R. Baldini Ferroli[20A], Y. Ban[31], D. W. Bennett[19], J. V. Bennett[5], N. B. Berger[22], M. Bertani[20A], D. Bettoni[21A], J. M. Bian[43], F. Bianchi[49A,49C], E. Boger[23,c], I. Boyko[23], R. A. Briere[5], H. Cai[51], X. Cai[1,a], O. Cakir[40A], A. Calcaterra[20A], G. F. Cao[1], S. A. Cetin[40B], J. F. Chang[1,a], G. Chelkov[23,c,d], G. Chen[1], H. S. Chen[1], H. Y. Chen[2], J. C. Chen[1], M. L. Chen[1,a], S. Chen[41], S. J. Chen[29], X. Chen[1,a], X. R. Chen[26], Y. B. Chen[1,a], H. P. Cheng[17], X. K. Chu[31], G. Cibinetto[21A], H. L. Dai[1,a], J. P. Dai[34], A. Dbeyssi[14], D. Dedovich[23], Z. Y. Deng[1], A. Denig[22], I. Denysenko[23], M. Destefanis[49A,49C], F. De Mori[49A,49C], Y. Ding[27], C. Dong[30], J. Dong[1,a], L. Y. Dong[1], M. Y. Dong[1,a], Z. L. Dou[29], S. X. Du[53], P. F. Duan[1], J. Z. Fan[39], J. Fang[1,a], S. S. Fang[1], X. Fang[46,a], Y. Fang[1], R. Farinelli[21A,21B], L. Fava[49B,49C], O. Fedorov[23], F. Feldbauer[22], G. Felici[20A], C. Q. Feng[46,a], E. Fioravanti[21A], M. Fritsch[14,22], C. D. Fu[1], Q. Gao[1], X. L. Gao[46,a], X. Y. Gao[2], Y. Gao[39], Z. Gao[46,a], I. Garzia[21A], K. Goetzen[10], L. Gong[30], W. X. Gong[1,a], W. Gradl[22], M. Greco[49A,49C], M. H. Gu[1,a], Y. T. Gu[12], Y. H. Guan[1], A. Q. Guo[1], L. B. Guo[28], R. P. Guo[1], Y. Guo[1], Y. P. Guo[22], Z. Haddadi[25], A. Hafner[22], S. Han[51], X. Q. Hao[15], F. A. Harris[42], K. L. He[1], F. H. Heinsius[4], T. Held[4], Y. K. Heng[1,a], T. Holtmann[4], Z. L. Hou[1], C. Hu[28], H. M. Hu[1], J. F. Hu[49A,49C], T. Hu[1,a], Y. Hu[1], G. S. Huang[46,a], J. S. Huang[15], X. T. Huang[33], X. Z. Huang[29], Y. Huang[29], Z. L. Huang[27], T. Hussain[48], Q. Ji[1], Q. P. Ji[30], X. B. Ji[1], X. L. Ji[1,a], L. W. Jiang[51], X. S. Jiang[1,a], X. Y. Jiang[30], J. B. Jiao[33], Z. Jiao[17], D. P. Jin[1,a], S. Jin[1], T. Johansson[50], A. Julin[43], N. Kalantar-Nayestanaki[25], X. L. Kang[1], X. S. Kang[30], M. Kavatsyuk[25], B. C. Ke[5], P. Kiese[22], R. Kliemt[14], B. Kloss[22], O. B. Kolcu[40B,h], B. Kopf[4], M. Kornicer[42], A. Kupsc[50], W. Kühn[24], J. S. Lange[24], M. Lara[19], P. Larin[14], H. Leithoff[22], C. Leng[49C], C. Li[50], Cheng Li[46,a], D. M. Li[53], F. Li[1,a], F. Y. Li[31], G. Li[1], H. B. Li[1], H. J. Li[1], J. C. Li[1], Jin Li[32], K. Li[13], K. Li[33], Lei Li[3], P. R. Li[41], Q. Y. Li[33], T. Li[33], W. D. Li[1], W. G. Li[1], X. L. Li[33], X. M. Li[12], X. N. Li[1,a], X. Q. Li[30], Y. B. Li[2], Z. B. Li[38], H. Liang[46,a], J. J. Liang[12], Y. F. Liang[36], Y. T. Liang[24], G. R. Liao[11], D. X. Lin[14], B. Liu[34], B. J. Liu[1], C. X. Liu[1], D. Liu[46,a], F. H. Liu[35], Fang Liu[1], Feng Liu[6], H. B. Liu[12], H. H. Liu[1], H. H. Liu[16], H. M. Liu[1], J. Liu[1], J. B. Liu[46,a], J. P. Liu[51], J. Y. Liu[1], K. Liu[39], K. Y. Liu[27], L. D. Liu[31], P. L. Liu[1,a], Q. Liu[41], S. B. Liu[46,a], X. Liu[26], Y. B. Liu[30], Y. Y. Liu[30], Z. A. Liu[1,a], Zhiqing Liu[22], H. Loehner[25], X. C. Lou[1,a,g], H. J. Lu[17], J. G. Lu[1,a], Y. Lu[1], Y. P. Lu[1,a], C. L. Luo[28], M. X. Luo[52], T. Luo[42], X. L. Luo[1,a], X. R. Lyu[41], F. C. Ma[27], H. L. Ma[1], L. L. Ma[33], M. M. Ma[1], Q. M. Ma[1], T. Ma[1], X. N. Ma[30], X. Y. Ma[1,a], Y. M. Ma[33], F. E. Maas[14], M. Maggiora[49A,49C], Q. A. Malik[48], Y. J. Mao[31], Z. P. Mao[1], S. Marcello[49A,49C], J. G. Messchendorp[25], G. Mezzadri[21B], J. Min[1,a], R. E. Mitchell[19], X. H. Mo[1,a], Y. J. Mo[6], C. Morales Morales[14], N. Yu. Muchnoi[9,e], H. Muramatsu[43], P. Musiol[4], Y. Nefedov[23], F. Nerling[14], I. B. Nikolaev[9,e], Z. Ning[1,a], S. Nisar[8], S. L. Niu[1,a], X. Y. Niu[1], S. L. Olsen[32], Q. Ouyang[1,a], S. Pacetti[20B], Y. Pan[46,a], P. Patteri[20A], M. Pelizaeus[4], H. P. Peng[46,a], K. Peters[10], J. Pettersson[50], J. L. Ping[28], R. G. Ping[1], R. Poling[43], V. Prasad[1], H. R. Qi[2], M. Qi[29], S. Qian[1,a], C. F. Qiao[41], L. Q. Qin[33], N. Qin[51], X. S. Qin[1], Z. H. Qin[1,a], J. F. Qiu[1], K. H. Rashid[48], C. F. Redmer[22], M. Ripka[22], G. Rong[1], Ch. Rosner[14], X. D. Ruan[12], A. Sarantsev[23,f], M. Savrié[21B], C. Schnier[4], K. Schoenning[50], S. Schumann[22], W. Shan[31], M. Shao[46,a], C. P. Shen[2], P. X. Shen[30], X. Y. Shen[1], H. Y. Sheng[1], M. Shi[1], W. M. Song[1], X. Y. Song[1], S. Sosio[49A,49C], S. Spataro[49A,49C], G. X. Sun[1], J. F. Sun[15], S. S. Sun[1], X. H. Sun[1], Y. J. Sun[46,a], Y. Z. Sun[1], Z. J. Sun[1,a], Z. T. Sun[19], C. J. Tang[36], X. Tang[1], I. Tapan[40C], E. H. Thorndike[44], M. Tiemens[25], I. Uman[40D], G. S. Varner[42], B. Wang[30], B. L. Wang[41], D. Wang[31], D. Y. Wang[31], K. Wang[1,a], L. L. Wang[1], L. S. Wang[1], M. Wang[33], P. Wang[1], P. L. Wang[1], S. G. Wang[31], W. Wang[1,a], W. P. Wang[46,a], X. F. Wang[39], Y. Wang[37], Y. D. Wang[14], Y. F. Wang[1,a], Y. Q. Wang[22], Z. Wang[1,a], Z. G. Wang[1,a], Z. H. Wang[46,a], Z. Y. Wang[1], Z. Y. Wang[1], T. Weber[22], D. H. Wei[11], J. B. Wei[31], P. Weidenkaff[22], S. P. Wen[1], U. Wiedner[4], M. Wolke[50], L. H. Wu[1], L. J. Wu[1], Z. Wu[1,a], L. Xia[46,a], L. G. Xia[39], Y. Xia[18], D. Xiao[1], H. Xiao[47], Z. J. Xiao[28], Y. G. Xie[1,a], Q. L. Xiu[1,a], G. F. Xu[1], J. J. Xu[1], L. Xu[1], Q. J. Xu[13], Q. N. Xu[41], X. P. Xu[37], L. Yan[49A,49C], W. B. Yan[46,a], W. C. Yan[46,a], Y. H. Yan[18], H. J. Yang[34], H. X. Yang[1], L. Yang[51], Y. X. Yang[11], M. Ye[1,a], M. H. Ye[7], J. H. Yin[1], B. X. Yu[1,a], C. X. Yu[30], J. S. Yu[26], C. Z. Yuan[1], W. L. Yuan[29], Y. Yuan[1], A. Yuncu[40B,b], A. A. Zafar[48], A. Zallo[20A], Y. Zeng[18], Z. Zeng[46,a], B. X. Zhang[1], B. Y. Zhang[1,a], C. Zhang[29], C. C. Zhang[1], D. H. Zhang[1], H. H. Zhang[38], H. Y. Zhang[1,a], J. Zhang[1], J. J. Zhang[1], J. L. Zhang[1], J. Q. Zhang[1], J. W. Zhang[1,a], J. Y. Zhang[1], J. Z. Zhang[1], K. Zhang[1], L. Zhang[1], S. Q. Zhang[30], X. Y. Zhang[33], Y. Zhang[1], Y. H. Zhang[1,a], Y. N. Zhang[41], Y. T. Zhang[46,a], Yu Zhang[41], Z. H. Zhang[6], Z. P. Zhang[46], Z. Y. Zhang[51], G. Zhao[1], J. W. Zhao[1,a], J. Y. Zhao[1], J. Z. Zhao[1,a], Lei Zhao[46,a], Ling Zhao[1], M. G. Zhao[30], Q. Zhao[1], Q. W. Zhao[1], S. J. Zhao[53], T. C. Zhao[1], Y. B. Zhao[1,a], Z. G. Zhao[46,a], A. Zhemchugov[23,c], B. Zheng[47], J. P. Zheng[1,a], W. J. Zheng[33], Y. H. Zheng[41], B. Zhong[28], L. Zhou[1,a], X. Zhou[51], X. K. Zhou[46,a], X. R. Zhou[46,a], X. Y. Zhou[1], K. Zhu[1], K. J. Zhu[1,a], S. Zhu[1], S. H. Zhu[45], X. L. Zhu[39], Y. C. Zhu[46,a], Y. S. Zhu[1], Z. A. Zhu[1], J. Zhuang[1,a], L. Zotti[49A,49C], B. S. Zou[1], J. H. Zou[1]

(BESIII Collaboration)

[1] *Institute of High Energy Physics, Beijing 100049, People's Republic of China*
[2] *Beihang University, Beijing 100191, People's Republic of China*
[3] *Beijing Institute of Petrochemical Technology, Beijing 102617, People's Republic of China*
[4] *Bochum Ruhr-University, D-44780 Bochum, Germany*
[5] *Carnegie Mellon University, Pittsburgh, Pennsylvania 15213, USA*
[6] *Central China Normal University, Wuhan 430079, People's Republic of China*
[7] *China Center of Advanced Science and Technology, Beijing 100190, People's Republic of China*
[8] *COMSATS Institute of Information Technology, Lahore, Defence Road, Off Raiwind Road, 54000 Lahore, Pakistan*
[9] *G.I. Budker Institute of Nuclear Physics SB RAS (BINP), Novosibirsk 630090, Russia*
[10] *GSI Helmholtzcentre for Heavy Ion Research GmbH, D-64291 Darmstadt, Germany*

[11] Guangxi Normal University, Guilin 541004, People's Republic of China
[12] GuangXi University, Nanning 530004, People's Republic of China
[13] Hangzhou Normal University, Hangzhou 310036, People's Republic of China
[14] Helmholtz Institute Mainz, Johann-Joachim-Becher-Weg 45, D-55099 Mainz, Germany
[15] Henan Normal University, Xinxiang 453007, People's Republic of China
[16] Henan University of Science and Technology, Luoyang 471003, People's Republic of China
[17] Huangshan College, Huangshan 245000, People's Republic of China
[18] Hunan University, Changsha 410082, People's Republic of China
[19] Indiana University, Bloomington, Indiana 47405, USA
[20] (A)INFN Laboratori Nazionali di Frascati, I-00044, Frascati, Italy; (B)INFN and University of Perugia, I-06100, Perugia, Italy
[21] (A)INFN Sezione di Ferrara, I-44122, Ferrara, Italy; (B)University of Ferrara, I-44122, Ferrara, Italy
[22] Johannes Gutenberg University of Mainz, Johann-Joachim-Becher-Weg 45, D-55099 Mainz, Germany
[23] Joint Institute for Nuclear Research, 141980 Dubna, Moscow region, Russia
[24] Justus-Liebig-Universitaet Giessen, II. Physikalisches Institut, Heinrich-Buff-Ring 16, D-35392 Giessen, Germany
[25] KVI-CART, University of Groningen, NL-9747 AA Groningen, The Netherlands
[26] Lanzhou University, Lanzhou 730000, People's Republic of China
[27] Liaoning University, Shenyang 110036, People's Republic of China
[28] Nanjing Normal University, Nanjing 210023, People's Republic of China
[29] Nanjing University, Nanjing 210093, People's Republic of China
[30] Nankai University, Tianjin 300071, People's Republic of China
[31] Peking University, Beijing 100871, People's Republic of China
[32] Seoul National University, Seoul, 151-747 Korea
[33] Shandong University, Jinan 250100, People's Republic of China
[34] Shanghai Jiao Tong University, Shanghai 200240, People's Republic of China
[35] Shanxi University, Taiyuan 030006, People's Republic of China
[36] Sichuan University, Chengdu 610064, People's Republic of China
[37] Soochow University, Suzhou 215006, People's Republic of China
[38] Sun Yat-Sen University, Guangzhou 510275, People's Republic of China
[39] Tsinghua University, Beijing 100084, People's Republic of China
[40] (A)Ankara University, 06100 Tandogan, Ankara, Turkey; (B)Istanbul Bilgi University, 34060 Eyup, Istanbul, Turkey; (C)Uludag University, 16059 Bursa, Turkey; (D)Near East University, Nicosia, North Cyprus, Mersin 10, Turkey
[41] University of Chinese Academy of Sciences, Beijing 100049, People's Republic of China
[42] University of Hawaii, Honolulu, Hawaii 96822, USA
[43] University of Minnesota, Minneapolis, Minnesota 55455, USA
[44] University of Rochester, Rochester, New York 14627, USA
[45] University of Science and Technology Liaoning, Anshan 114051, People's Republic of China
[46] University of Science and Technology of China, Hefei 230026, People's Republic of China
[47] University of South China, Hengyang 421001, People's Republic of China
[48] University of the Punjab, Lahore-54590, Pakistan
[49] (A)University of Turin, I-10125, Turin, Italy; (B)University of Eastern Piedmont, I-15121, Alessandria, Italy; (C)INFN, I-10125, Turin, Italy
[50] Uppsala University, Box 516, SE-75120 Uppsala, Sweden
[51] Wuhan University, Wuhan 430072, People's Republic of China
[52] Zhejiang University, Hangzhou 310027, People's Republic of China
[53] Zhengzhou University, Zhengzhou 450001, People's Republic of China

[a] Also at State Key Laboratory of Particle Detection and Electronics, Beijing 100049, Hefei 230026, People's Republic of China
[b] Also at Bogazici University, 34342 Istanbul, Turkey
[c] Also at the Moscow Institute of Physics and Technology, Moscow 141700, Russia
[d] Also at the Functional Electronics Laboratory, Tomsk State University, Tomsk, 634050, Russia
[e] Also at the Novosibirsk State University, Novosibirsk, 630090, Russia
[f] Also at the NRC "Kurchatov Institute, PNPI, 188300, Gatchina, Russia
[g] Also at University of Texas at Dallas, Richardson, Texas 75083, USA
[h] Also at Istanbul Arel University, 34295 Istanbul, Turkey

We present an amplitude analysis of the decay $D^0 \to K^-\pi^+\pi^+\pi^-$ based on a data sample of 2.93 fb^{-1} acquired by the BESIII detector at the $\psi(3770)$ resonance. With a nearly background free sample of about 16000 events, we investigate the substructure of the decay and determine the relative fractions and the phases among the different intermediate processes. Our amplitude model includes the two-body decays $D^0 \to \bar{K}^{*0}\rho^0$, $D^0 \to K^- a_1^+(1260)$ and $D^0 \to K_1^-(1270)\pi^+$, the three-

body decays $D^0 \to \bar{K}^{*0}\pi^+\pi^-$ and $D^0 \to K^-\pi^+\rho^0$, as well as the four-body non-resonant decay $D^0 \to K^-\pi^+\pi^+\pi^-$. The dominant intermediate process is $D^0 \to K^- a_1^+(1260)$, accounting for a fit fraction of 54.6%.

PACS numbers: 13.20.Ft, 14.40.Lb

I. INTRODUCTION

The decay $D^0 \to K^-\pi^+\pi^+\pi^-$ is one of the three golden decay modes of the neutral D meson (the other two are $D^0 \to K^-\pi^+$ and $D^0 \to K^-\pi^+\pi^0$). Due to a large branching fraction and low background it is well suited to used as a reference channel for other decays of the D^0 meson [1]. An accurate knowledge of its resonant substructure and the relative amplitudes and phases are important to reduce systematic uncertainties in analyses that use this channel for reference. In particular, the lack of knowledge of the substructure leads to one of the largest systematic uncertainties in the measurement of the absolute branching fractions of the D hadronic decays [2]. The knowledge of the decay substructure in combination with a precise measurement of strong phases can also help to improve the measurement of the CKM angle γ [3]. In the measurement of γ, the parameterization model is an important input information in a model dependent method and also can be used to generate Monte Carlo (MC) to check the sensitivity in a model independent method [4]. Furthermore, the branching fractions of intermediate processes can be used to understand the $D^0 - \bar{D}^0$ mixing in theory [5, 6].

The decay $D^0 \to K^-\pi^+\pi^+\pi^-$ was studied by Mark III [7] and E691 [8] more than twenty years ago. Both measurements are affected by low statistics. Using about 1300 signal events, Mark III obtained the branching fractions for $D^0 \to K^- a_1^+(1260)$, $D^0 \to \bar{K}^{*0}\rho^0$, $D^0 \to K_1^-(1270)\pi^+$, as well as for the three- and four-body non-resonant decays. Based on 1745 signal events and 800 background events, E691 obtained a similar result but without considering the $D^0 \to K_1^-(1270)\pi^+$ decay mode. The results from Mark III and E691 have large uncertainties. Therefore, further experimental study of $D^0 \to K^-\pi^+\pi^+\pi^-$ decay is of great importance for improving the precision of future measurements.

In this paper, a data sample of about 2.93 fb^{-1} [9, 10] collected at the $\psi(3770)$ resonance with the BESIII detector in 2010 and 2011 is used. We perform an amplitude analysis of the decay $D^0 \to K^-\pi^+\pi^+\pi^-$ (the inclusion of charge conjugate reactions is implied) to study the resonant substructure in this decay. The $\psi(3770)$ decays into a $D^0\bar{D}^0$ pair without any additional hadrons. We employ a double-tag method to measure the branching fraction. In order to suppress the backgrounds from other charmed meson decays and continuum (QED and $q\bar{q}$) processes, only the decay mode $\bar{D}^0 \to K^+\pi^-$ is used to tag the $D^0\bar{D}^0$ pair. A detailed discussion of background can be found in Sec. III. The amplitude model is constructed using the covariant tensor formalism [11].

II. DETECTION AND DATA SETS

The BESIII detector is described in detail in Ref. [12]. The geometrical acceptance of the BESIII detector is 93% of the full solid angle. Starting from the interaction point (IP), it consists of a main drift chamber (MDC), a time-of-flight (TOF) system, a CsI(Tl) electromagnetic calorimeter (EMC) and a muon system (MUC) with layers of resistive plate chambers (RPC) in the iron return yoke of a 1.0 T superconducting solenoid. The momentum resolution for charged tracks in the MDC is 0.5% at a transverse momentum of 1 GeV/c.

Monte Carlo (MC) simulations are based on GEANT4 [13]. The production of $\psi(3770)$ is simulated with the KKMC [14] package, taking into account the beam energy spread and initial-state radiation (ISR). The PHOTOS [15] package is used to simulate the final-state radiation (FSR) of charged tracks. The MC samples, which consist of $\psi(3770)$ decays to $D\bar{D}$, non-$D\bar{D}$, ISR production of low mass charmonium states and continuum processes, are referred to as "generic MC". The EvtGen [16] package is used to simulate the known decay modes with branching fractions taken from the Particle Data Group (PDG) [1], and the remaining unknown decays are generated with the LundCharm model [17]. The effective luminosities of the generic MC samples correspond to at least five times the data sample luminosity. They are used to investigate possible backgrounds. The decay $D^0 \to K_S^0(\pi^+\pi^-)K^-\pi^+$ has the same final state as signal and is investigated using a dedicated MC sample with the decay chain of $\psi(3770) \to D^0\bar{D}^0$ with $D^0 \to K_S^0K^-\pi^+$ and $\bar{D}^0 \to K^+\pi^-$, referred to as "$K_S^0K\pi$ MC". The decay model of $D^0 \to K_S^0K^-\pi^+$ is generated according to CLEO's results [18]. In amplitude analysis, two sets of signal MC samples using different decay models are generated. One sample is generated with an uniform distribution in phase space for the $D^0 \to K^-\pi^+\pi^+\pi^-$ decay, which is used in calculate the MC integrations and called "PHSP MC". The other sample is generated according to the results obtained in this analysis for the $D^0 \to K^-\pi^+\pi^+\pi^-$ decay. It is used to check the fit performance, calculate the goodness of fit and estimate the detector efficiency, and is called the "SIGNAL MC".

III. EVENT SELECTION

Good charged tracks are required to have a point of closest approach to the interaction point (IP) within 10

cm along the beam axis and within 1 cm in the plane perpendicular to beam. The polar angle θ between the track and the e^+ beam direction is required to satisfy $|\cos\theta| < 0.93$. Charged particle identification (PID) is implemented by combining the energy loss (dE/dx) in the MDC and the time-of-fight information from the TOF. Probabilities $P(K)$ and $P(\pi)$ with the hypotheses of K or π are then calculated. Tracks without PID information are rejected. Charged kaon candidates are required to have $P(K) > P(\pi)$, while the π candidates are required to have $P(\pi) > P(K)$. The average efficiencies for the kaon and pions in $K^-\pi^+\pi^+\pi^-$ are $\sim 98\%$ and $\sim 99\%$ respectively. The $D^0\bar{D}^0$ pair with $\bar{D}^0 \to K^+\pi^-$ and $D^0 \to K^-\pi^+\pi^+\pi^-$ is reconstructed with the requirement that the two D^0 mesons have opposite charm and do not have any tracks in common. Since the tracks in $K^-\pi^+\pi^+\pi^-$ have distinct momenta from those in $K^+\pi^-$, misreconstructed signal events and K/π particle misidentification are negligible. Furthermore, a vertex fit with the hypothesis that all tracks originate from the IP is performed, and the χ^2 of the fit is required to be less than 200.

For the $K^+\pi^-$ and $K^-\pi^+\pi^+\pi^-$ combinations, two variables, $M_{\rm BC}$ and ΔE, are calculated:

$$M_{\rm BC} \equiv \sqrt{E^2_{\rm beam} - \vec{p}^2_D}, \tag{1}$$

and

$$\Delta E \equiv E_D - E_{\rm beam}, \tag{2}$$

where $\vec{p}_D$ and E_D are the reconstructed momentum and energy of a D candidate, $E_{\rm beam}$ is the calibrated beam energy. The signal events form a peak around zero in the ΔE distribution and around the D^0 mass in the $M_{\rm BC}$ distribution. We require $-0.03 < \Delta E < 0.03$ GeV for the $K^+\pi^-$ final state, $-0.033 < \Delta E < 0.033$ GeV for the $K^-\pi^+\pi^+\pi^-$ final state and $1.8575 < M_{\rm BC} < 1.8775$ GeV/c^2 for both of them. The corresponding ΔE and $M_{\rm BC}$ of selected candidate are shown in Fig. 1, where the background is negligible.

To ensure the D^0 meson is on shell and improve the resolution, the selected candidate events are further subjected to a five-constraint (5C) kinematic fit, which constrains the total four-momentum of all final state particles to the initial four-momentum of the e^+e^- system, and the invariant mass of signal side $K^-\pi^+\pi^+\pi^-$ constrains to the D^0 mass in PDG [1]. We discard events with a χ^2 of the 5C kinematic fit larger than 40. In order to suppress the background of $D^0 \to K^0_S K^-\pi^+$ with $K^0_S \to \pi^+\pi^-$, which has the same final state as our signal decay, we perform a vertex constrained fit on any $\pi^+\pi^-$ pair in the signal side if the $\pi^+\pi^-$ invariant mass falls into the mass window $|m_{\pi^+\pi^-} - m_{K^0_S}| < 0.03$ GeV/c^2 ($m_{K^0_S}$ is the K^0_S nominal mass [1]), and reject the event if the corresponding significance of decay length (*e.g.* the distance of the decay vertex to IP) is larger than 2σ. The K^0_S veto eliminates about 80% $D^0 \to K^0_S K^-\pi^+$ background while retaining about 99% of signal events. After applying all selection criteria, 15912 candidate events are obtained with a purity of 99.4%, as estimated by MC simulation.

The MC studies indicate that the dominant background arises from the $D^0 \to K^0_S K^-\pi^+$ decay, the corresponding produced number of events is estimated according to

$$N(K^0_S K^-\pi^+|K^+\pi^-) = \frac{Y(K^-\pi^+\pi^+\pi^-|K^+\pi^-)}{\epsilon(K^-\pi^+\pi^+\pi^-|K^+\pi^-)} \times \frac{\mathcal{B}(K^0_S K^-\pi^+)}{\mathcal{B}(K^-\pi^+\pi^+\pi^-)}, \tag{3}$$

where $N(K^0_S K^-\pi^+|K^+\pi^-)$ is the production of $\psi(3770) \to D^0\bar{D}^0$ with $D^0 \to K^0_S K^-\pi^+$ and $\bar{D}^0 \to K^+\pi^-$, $Y(K^-\pi^+\pi^+\pi^-|K^+\pi^-)$ is the signal yield with background subtracted but without efficiency correction applied and ϵ is the corresponding efficiency obtained from SIGNAL MC, which is generated according to the results of fit to data whose peaking background estimated from generic MC. $\mathcal{B}(K^-\pi^+\pi^+\pi^-)$ and $\mathcal{B}(K^0_S K^-\pi^+)$ are the branching fractions for $D^0 \to K^-\pi^+\pi^+\pi^-$ and $D^0 \to K^0_S K^-\pi^+$, respectively, which are quoted from the PDG [1]. According to Eq. (3), the number of peaking background events ($N_{\rm peaking}$) is estimated to be 96.8 ± 14.5.

All other backgrounds from $D\bar{D}$, $q\bar{q}$ and non-$D\bar{D}$ decays are studied with the generic MC sample. Their total contribution is estimated to be less than 10 events, of which 5.5 and 2.0 are from the $D^0\bar{D}^0$ decays and the non-$D\bar{D}$ decays, respectively. These backgrounds are neglected in the following analysis and their effect is considered as a systematic uncertainty, as discussed in Sec. VI 2.

IV. AMPLITUDE ANALYSIS

The decay modes which may contribute to the $D^0 \to K^-\pi^+\pi^+\pi^-$ decay are listed in Table I, where the symbols S, P, V, A, and T denote a scalar, pseudoscalar, vector, axial-vector, and tensor state, respectively. The letters S, P, and D in square brackets refer to the relative angular momentum between the daughter particles. The amplitudes and the relative phases between the different decay modes are determined with a maximum likelihood fit.

A. Likelihood Function Construction

The likelihood function is the product of the probability density function (PDF) of the observed events. The signal PDF $f_S(p_j)$ is given by

$$f_S(p_j) = \frac{\epsilon(p_j)|M(p_j)|^2 R_4(p_j)}{\int \epsilon(p_j)|M(p_j)|^2 R_4(p_j) dp_j}, \tag{4}$$

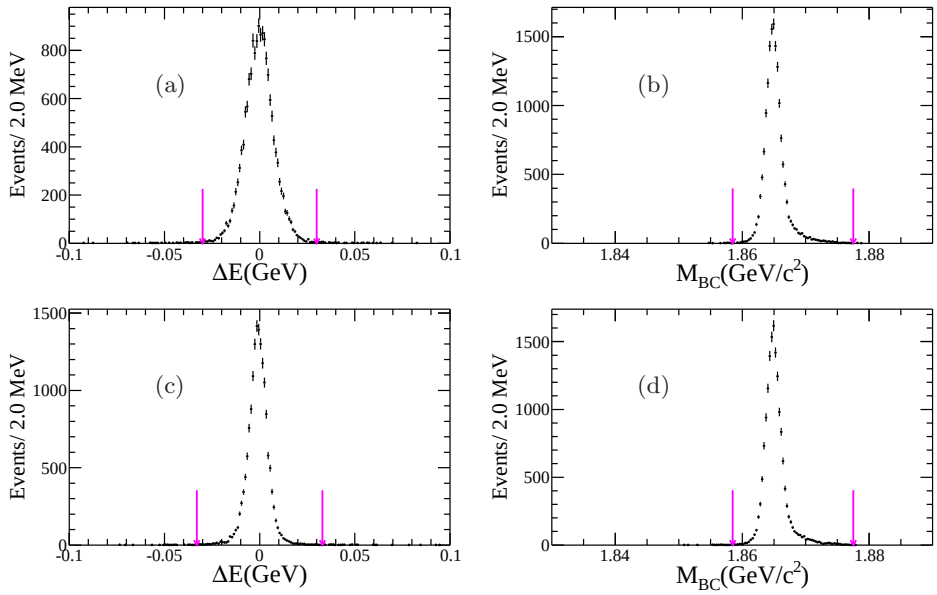

FIG. 1. Distributions of data for ΔE ((a) and (c)) and $M_{\rm BC}$ ((b) and (d)) in $K^+\pi^-$ side ((a) and (b)) and in $K^-\pi^+\pi^+\pi^-$ side ((c) and (d)). The arrows indicate the selection criteria. In each plot, all selection criteria described in this section have been applied except the one on the variable.

where $\epsilon(p_j)$ is the detection efficiency parameterized in terms of the final four-momenta p_j. The index j refers to the different particles in the final state. $R_4(p_j)dp_j$ is the standard element of the four-body phase space [11], which is given by

$$R_4(p_j)dp_j = \delta^4\left(p_{D^0} - \sum_{j=1}^{4} p_j\right)\prod_{j=1}^{4}\frac{d^3\mathbf{p}_j}{(2\pi)^3 2E_j}. \quad (5)$$

$M(p_j)$ is the total decay amplitude which is modeled as a coherent sum over all contributing amplitudes

$$M(p_j) = \sum_n c_n A_n(p_j), \quad (6)$$

where the complex coefficient $c_n = \rho_n e^{i\phi_n}$ (ρ_n and ϕ_n are the magnitude and phase for the $n^{\rm th}$ amplitude, respectively) and $A_n(p_j)$ describe the relative contribution and the dynamics of the $n^{\rm th}$ amplitude. In four-body decays, the intermediate amplitude can be a quasi-two-body decay or a cascade decay amplitude, and $A_n(p_j)$ is given by

$$A_n(p_j) = P_n^1(m_1)P_n^2(m_2)S_n(p_j)F_n^1(p_j)F_n^2(p_j)F_n^D(p_j), \quad (7)$$

where the indices 1 and 2 correspond to the two intermediate resonances. Here, $P_n^\alpha(m_\alpha)$ and $F_n^\alpha(p_j)$ ($\alpha = 1, 2$) are the propagator and the Blatt-Weisskopf barrier factor [19], respectively, and $F_n^D(p_j)$ is the Blatt-Weisskopf barrier factor of the D^0 decay. The parameters m_1 and m_2 in the propagators are the invariant masses of the corresponding systems. For non-resonant states with orbital angular momentum between the daughters, we set the propagator to unity, which can be regarded as a very broad resonance. The spin factor $S_n(p_j)$ is constructed with the covariant tensor formalism [11]. In practice, the presence of the two π^+ mesons imposes a Bose symmetry in the $K^-\pi^+\pi^+\pi^-$ final state. This symmetry is explicitly accounted for in the amplitude by exchange of the two pions with the same charge.

The contribution from the background is subtracted in the likelihood calculation by assigning a negative weight to the background events

$$\ln L = \sum_{k=1}^{N_{\rm data}} \ln f_S(p_j^k) - \sum_{k'=1}^{N_{\rm bkg}} w_{k'}^{\rm bkg} \ln f_S(p_j^{k'}), \quad (8)$$

where $N_{\rm data}$ is the number of candidate events in data, $w_{k'}^{\rm bkg}$ and $N_{\rm bkg}$ are the weight and the number of events from the background MC sample, respectively. In the nominal fit, only the peaking background $D^0 \to K_S^0 K^-\pi^+$ is considered, and the weight $w_{k'}^{\rm bkg}$ is fixed to $N_{\rm peaking}/N_{\rm bkg}$. p_j^k and $p_j^{k'}$ are the four-momenta of the j^{th} final particle in the k^{th} event of the data sample and in the k'^{th} event of the background MC sample, respectively.

The normalization integral is determined by a MC technique taking into account the difference of detector efficiencies for PID and tracking between data and MC simulation. The weight for a given MC event is defined as

$$\gamma_\epsilon(p_j) = \prod_j \frac{\epsilon_{j,\rm data}(p_j)}{\epsilon_{j,\rm MC}(p_j)}, \quad (9)$$

where $\epsilon_{j,\rm data}(p_j)$ and $\epsilon_{j,\rm MC}(p_j)$ are the PID or tracking efficiencies for charged tracks as a function of p_j for the data and MC sample, respectively. The efficiencies $\epsilon_{j,\rm data}(p_j)$ and $\epsilon_{j,\rm MC}(p_j)$ are determined by studying the $D^0 \to K^-\pi^+\pi^+\pi^-$ sample for data and MC respectively. The MC integration is then given by

$$\begin{aligned}&\int \epsilon(p_j)|M(p_j)|^2 R_4(p_j)dp_j \\ &= \frac{1}{N_{\rm MC}}\sum_{k_{\rm MC}}^{N_{\rm MC}} \frac{|M(p_j^{k_{\rm MC}}))|^2\gamma_\epsilon(p_j^{k_{\rm MC}})}{|M^{\rm gen}(p_j^{k_{\rm MC}})|^2},\end{aligned} \tag{10}$$

where $k_{\rm MC}$ is the index of the $k_{\rm MC}^{th}$ event of the MC sample and $N_{\rm MC}$ is the number of the selected MC events. $M^{\rm gen}(p_j)$ is the PDF function used to generate the MC samples in MC integration. In the numerator of Eq. (4), $\epsilon(p_j)$ is independent of the fitted variables, so it is regarded as a constant term in the fit.

1. Spin Factors

Due to the limited phase space available in the decay, we only consider the states with angular momenta up to 2. As discussed in Ref. [11], we define the spin projection operator $P^{(S)}_{\mu_1\cdots\mu_S\nu_1\cdots\nu_S}$ for a process $a \to bc$ as

$$P^{(1)}_{\mu\nu} = -g_{\mu\nu} + \frac{p_{a\mu}p_{a\nu}}{p_a^2} \tag{11}$$

for spin 1,

$$\begin{aligned}&P^{(2)}_{\mu_1\mu_2\nu_1\nu_2} = \\ &\frac{1}{2}(P^{(1)}_{\mu_1\nu_1}P^{(1)}_{\mu_2\nu_2} + P^{(1)}_{\mu_1\nu_2}P^{(1)}_{\mu_2\nu_1}) - \frac{1}{3}P^{(1)}_{\mu_1\mu_2}P^{(1)}_{\nu_1\nu_2}\end{aligned} \tag{12}$$

for spin 2. The covariant tensors $\tilde{t}^L_{\mu_1\cdots\mu_l}$ for the final states of pure orbital angular momentum L are constructed from relevant momenta p_a, p_b, p_c [11]

$$\tilde{t}^L_{\mu_1\cdots\mu_L} = (-1)^L P^{(L)}_{\mu_1\cdots\mu_L\nu_1\cdots\nu_L} r^{\nu_1}\cdots r^{\nu_L}, \tag{13}$$

where $r = p_b - p_c$.

Ten kinds of decay modes used in the analysis are listed in Table I. We use $\tilde{T}^{(L)}_{\mu_1\ldots\mu_L}$ to represent the decay from the D meson and $\tilde{t}^{(L)}_{\mu_1\ldots\mu_L}$ to represent the decay from the intermediate state.

2. Blatt-Weisskopf Barrier Factors

The Blatt-Weisskopf barrier factor [19] $F_L(p_j)$ is a function of the angular momentum L and the four-momenta p_j of the daughter particles. For a process $a \to bc$, the magnitude of the momentum q of the daughter b or c in the rest system of a is given by

$$q = \sqrt{\frac{(s_a + s_b - s_c)^2}{4s_a} - s_b} \tag{14}$$

with $s_\beta = E_\beta^2 - \vec{p}_\beta^2, \beta = a, b, c$. The Blatt-Weisskopf barrier factor is then given by

$$F_L(q) = z^L X_L(q), \tag{15}$$

where $z = qR$. R is the effective radius of the barrier, which is fixed to $3.0\,\mathrm{GeV}^{-1}$ for intermediate resonances and $5.0\,\mathrm{GeV}^{-1}$ for the D^0 meson. $X_L(q)$ is given by

$$X_{L=0}(q) = 1, \tag{16}$$

$$X_{L=1}(q) = \sqrt{\frac{2}{z^2+1}}, \tag{17}$$

$$X_{L=2}(q) = \sqrt{\frac{13}{z^4+3z^2+9}}. \tag{18}$$

3. Propagator

The resonances $\bar{K}^{*0}$ and $a_1^+(1260)$ are parameterized as relativistic Breit-Wigner function with a mass depended width

$$P(m) = \frac{1}{(m_0^2 - s_a) - im_0\Gamma(m)}, \tag{19}$$

where m_0 is the mass of resonance to be determined. $\Gamma(m)$ is given by

$$\Gamma(m) = \Gamma_0\left(\frac{q}{q_0}\right)^{2L+1}\left(\frac{m_0}{m}\right)\left(\frac{X_L(q)}{X_L(q_0)}\right)^2, \tag{20}$$

where q_0 denotes the value of q at $m = m_0$. The $K_1^-(1270)$ is parameterized as a relativistic Breit-Wigner function with a constant width $\Gamma(m) = \Gamma_0$ and the ρ^0 is parameterized with the Gounaris-Sakurai line-shape [20], which is given by

$$P_{\rm GS}(m) = \frac{1 + d\frac{\Gamma_0}{m_0}}{(m_0^2 - m^2) + f(m) - im_0\Gamma(m)}, \tag{21}$$

where

$$\begin{aligned}f(m) = \Gamma_0\frac{m_0^2}{q_0^3}\Big[&q^2(h(m) - h(m_0)) \\ &+(m_0^2 - m^2)q_0^2\frac{dh}{d(m^2)}\Big|_{m^2=m_0^2}\Big],\end{aligned} \tag{22}$$

and the function $h(m)$ is defined as

$$h(m) = \frac{2}{\pi}\frac{q}{m}\ln\left(\frac{m + 2q}{2m_\pi}\right), \tag{23}$$

TABLE I. Spin factors $S(p)$ for different decay modes.

Decay mode	$S(p)$
$D[S] \to \mathrm{V}_1\,\mathrm{V}_2,\ \mathrm{V}_1 \to \mathrm{P}_1\,\mathrm{P}_2,\ \mathrm{V}_2 \to \mathrm{P}_3\,\mathrm{P}_4$	$\tilde{t}^{(1)\mu}(\mathrm{V}_1)\tilde{t}^{(1)}_{\mu}(\mathrm{V}_2)$
$D[P] \to \mathrm{V}_1\,\mathrm{V}_2,\ \mathrm{V}_1 \to \mathrm{P}_1\,\mathrm{P}_2,\ \mathrm{V}_2 \to \mathrm{P}_3\,\mathrm{P}_4$	$\epsilon_{\mu\nu\lambda\sigma}p^{\mu}(D)\tilde{T}^{(1)\nu}(D)\tilde{t}^{(1)\lambda}(\mathrm{V}_1)\tilde{t}^{(1)\sigma}(\mathrm{V}_2)$
$D[D] \to \mathrm{V}_1\,\mathrm{V}_2,\ \mathrm{V}_1 \to \mathrm{P}_1\,\mathrm{P}_2,\ \mathrm{V}_2 \to \mathrm{P}_3\,\mathrm{P}_4$	$\tilde{T}^{(2)\mu\nu}(D)\tilde{t}^{(1)}_{\mu}(\mathrm{V}_1)\tilde{t}^{(1)}_{\nu}(\mathrm{V}_2)$
$D \to \mathrm{AP}_1,\ \mathrm{A}[S] \to \mathrm{VP}_2,\ \mathrm{V} \to \mathrm{P}_3\,\mathrm{P}_4$	$\tilde{T}^{\mu}_{1}(D)P^{(1)}_{\mu\nu}(\mathrm{A})\tilde{t}^{(1)\nu}(\mathrm{V})$
$D \to \mathrm{AP}_1,\ \mathrm{A}[D] \to \mathrm{VP}_2,\ \mathrm{V} \to \mathrm{P}_3\,\mathrm{P}_4$	$\tilde{T}^{(1)\mu}(D)\tilde{t}^{(2)}_{\mu\nu}(\mathrm{A})\tilde{t}^{(1)\nu}(\mathrm{V})$
$D \to \mathrm{AP}_1,\ \mathrm{A} \to \mathrm{SP}_2,\ \mathrm{S} \to \mathrm{P}_3\,\mathrm{P}_4$	$\tilde{T}^{(1)\mu}(D)\tilde{t}^{(1)}_{\mu}(\mathrm{A})$
$D \to \mathrm{VS},\ \mathrm{V} \to \mathrm{P}_1\,\mathrm{P}_2,\ \mathrm{S} \to \mathrm{P}_3\,\mathrm{P}_4$	$\tilde{T}^{(1)\mu}(D)\tilde{t}^{(1)}_{\mu}(\mathrm{V})$
$D \to \mathrm{V}_1\,\mathrm{P}_1,\ \mathrm{V}_1 \to \mathrm{V}_2\,\mathrm{P}_2,\ \mathrm{V}_2 \to \mathrm{P}_3\,\mathrm{P}_4$	$\epsilon_{\mu\nu\lambda\sigma}p^{\mu}_{\mathrm{V}_1}q^{\nu}_{\mathrm{V}_1}p^{\lambda}_{\mathrm{P}_1}q^{\sigma}_{\mathrm{V}_2}$
$D \to \mathrm{PP}_1,\ \mathrm{P} \to \mathrm{VP}_2,\ \mathrm{V} \to \mathrm{P}_3\,\mathrm{P}_4$	$p^{\mu}(\mathrm{P}_2)\tilde{t}^{(1)}_{\mu}(\mathrm{V})$
$D \to \mathrm{TS},\ \mathrm{T} \to \mathrm{P}_1\,\mathrm{P}_2,\ \mathrm{S} \to \mathrm{P}_3\,\mathrm{P}_4$	$\tilde{T}^{(2)\mu\nu}(D)\tilde{t}^{(2)}_{\mu\nu}(\mathrm{T})$

with

$$\left.\frac{dh}{d(m^2)}\right|_{m^2=m_0^2} = h(m_0)[(8q_0^2)^{-1} - (2m_0^2)^{-1}] + (2\pi m_0^2)^{-1} \quad (24)$$

where m_π is the charged pion mass. The normalization condition at $P_{\mathrm{GS}}(0)$ fixes the parameter $d = f(0)/(\Gamma_0 m_0)$. It is found to be [20]

$$d = \frac{3}{\pi}\frac{m_\pi^2}{q_0^2}\ln\left(\frac{m_0+2q_0}{2m_\pi}\right) + \frac{m_0}{2\pi q_0} - \frac{m_\pi^2 m_0}{\pi q_0^3}. \quad (25)$$

4. Parameterization of the $K\pi$ S-Wave

For the $K\pi$ S-wave (denoted as $(K\pi)_{\mathrm{S-wave}}$), we use the same parameterization as BABAR [21], which is extracted from scattering data [22]. The model is built from a Breit-Wigner shape for the $\bar{K}_0^*(1430)^0$ combined with an effective range parameterization for the non-resonant component given by

$$A(m_{K\pi}) = F\sin\delta_F e^{i\delta_F} + R\sin\delta_R e^{i\delta_R}e^{i2\delta_F}, \quad (26)$$

with

$$\delta_F = \phi_F + \cot^{-1}\left[\frac{1}{aq} + \frac{rq}{2}\right], \quad (27)$$

$$\delta_R = \phi_R + \tan^{-1}\left[\frac{M\Gamma(m_{K\pi})}{M^2 - m_{K\pi}^2}\right], \quad (28)$$

where a and r denote the scattering length and effective interaction length. F (ϕ_F) and R (ϕ_R) are the relative magnitudes (phases) for the non-resonant and resonant terms, respectively. q and $\Gamma(m_{K\pi})$ are defined as in Eq. (14) and Eq. (20), respectively. In the fit, the parameters M, Γ, F, ϕ_F, R, ϕ_R, a and r are fixed to the values obtained from the fit to the $D^0 \to K^0_S\pi^+\pi^-$ Dalitz Plot [21], as summarized in Table II. These fixed parameters will be varied within their uncertainties to estimate the corresponding systematic uncertainties, which is discussed in detail in Sec. VI 1.

TABLE II. $K\pi$ S-wave parameters, obtained from the fit to the $D^0 \to K^0_S\pi^+\pi^-$ Dalitz plot from BABAR [21].

$M(\mathrm{GeV}/c^2)$	1.463 ± 0.002
$\Gamma(\mathrm{GeV}/c^2)$	0.233 ± 0.005
F	0.80 ± 0.09
ϕ_F	2.33 ± 0.13
R	1(fixed)
ϕ_R	-5.31 ± 0.04
a	1.07 ± 0.11
r	-1.8 ± 0.3

B. Fit Fraction and the Statistical Uncertainty

We divide the fit model into several components according to the intermediate resonances, which can be found in Sec. V. The fit fractions of the individual components (amplitudes) are calculated according to the fit results and are compared to other measurements. In the calculation, a large phase space (PHSP) MC sample with neither detector acceptance nor resolution involved is used. The fit fraction for an amplitude or a component (a certain subset of amplitudes) is defined as

$$FF(n) = \frac{\sum_{k=1}^{N_{\mathrm{gen}}}|\tilde{A}_{\mathbf{n}}(p_j^k)|^2}{\sum_{k=1}^{N_{\mathrm{gen}}}|M(p_j^k)|^2}, \quad (29)$$

where $\tilde{A}_{\mathbf{n}}(p_j^k)$ is either the n^{th} amplitude ($\tilde{A}_{\mathbf{n}}(p_j^k) = c_n A_n(p_j^k)$) or the $\mathbf{n}^{th}$ component of a coherent sum of amplitudes ($\tilde{A}_{\mathbf{n}}(p_j^k) = \sum c_{n_i}A_{n_i}(p_j^k)$), N_{gen} is the number of the PHSP MC events.

To estimate the statistical uncertainties of the fit fractions, we repeat the calculation of fit fractions by randomly varying the fitted parameters according to the error matrix. Then, for every amplitude or component, we fit the resulting distribution with a Gaussian function, whose width gives the corresponding statistical uncertainty.

C. Goodness of Fit

To examine the performance of the fit process, the goodness of fit is defined as follows. Since the D^0 and all four final states particles have spin zero, the phase space of the decay $D^0 \to K^-\pi^+\pi^+\pi^-$ can be completely described by five linearly independent Lorentz invariant variables. Denoting as π_1^+ the one of the two identical pions which results in a higher $\pi^+\pi^-$ invariant mass and the other pion as π_2^+, we choose the five invariant masses $m_{\pi_1^+\pi^-}$, $m_{\pi_2^+\pi^-}$, $m_{K^-\pi_1^+\pi^-}$, $m_{\pi_1^+\pi_2^+\pi^-}$ and $m_{K^-\pi_1^+\pi_2^+}$. To calculate the goodness of fit, the five-dimensional phase space is first divided into cells with equal size. Then, adjacent cells are combined until the number of events in each cell is larger than 20. The deviation of the fit in each cell is calculated, $\chi_p = \frac{N_p - N_p^{\rm exp}}{\sqrt{N_p^{\rm exp}}}$, and the goodness of fit is quantified as $\chi^2 = \sum_{p=1}^{n} \chi_p^2$, where N_p and $N_p^{\rm exp}$ are the number of the observed events and the expected number determined from the fit results in the p^{th} cell, respectively, and n is the total number of cells. The number of degrees of freedom (NDF) ν is given by $\nu = (n-1) - n_{\rm par}$, where $n_{\rm par}$ is the number of the free parameters in the fit.

V. RESULTS

In order to determine the optimal set of amplitude that contribute to the decay $D^0 \to K^-\pi^+\pi^+\pi^-$, considering the results in PDG [1], we start with the fit including the components with significant contribution and add more amplitude in the fit one by one. The corresponding statistical significance for the new amplitude is calculated with the change of the log likelihood value $\Delta \ln L$, taking the change of the degrees of freedom $\Delta\nu$ into account.

In the $K^-\pi^+$ and $\pi^+\pi^-$ invariant mass spectra, there are clear structures for $\bar{K}^{*0}$ and ρ^0. The intermediate resonance $K_1^-(1270)$ is observed with $K_1^-(1270) \to \bar{K}^{*0}\pi^-$ or $K^-\rho^0$. In the $\pi^+\pi^+\pi^-$ invariant mass spectrum, a broad bump appears. We find this bump can be fitted as $a_1^+(1260)$, which was also observed by the Mark III [7] experiment. If it is fitted with a non-resonant $(\rho^0\pi^+)_{\rm A}$ amplitude instead, we find that the significance for $a_1^+(1260)$ with respect to $(\rho^0\pi^+)_{\rm A}$ is larger than 10σ. The three-body non-resonant states come from two kinds of contributions, $K^-\pi^+\rho^0$ and $\bar{K}^{*0}\pi^+\pi^-$. The $\bar{K}^{*0}\pi^-/K^-\rho^0$ can be in a pseudoscalar, a vector or an axial-vector state, while the $K^-\pi^+/\pi^+\pi^-$ can be in a scalar state. The four-body non-resonant states are relatively complex, such as $D \to$ VV, $D \to$ VS, $D \to$ TS, $D \to$ TV, $D \to$ AP with A $\to$ VP or SP, all of which may contribute to the decay. Since the process $D^0 \to K^-a_1^+(1260)$, $a_1^+(1260)[S] \to \rho^0\pi^+$ has the largest fit fraction, we fix the corresponding magnitude and phase to 1.0 and 0.0 and allow the magnitudes and phases of the other processes to vary in the fit.

We keep the processes with significance larger than 5σ for the next iteration. The fit involving both the $K^-a_1^+(1260)$ and the non-resonant $K^-(\rho^0\pi^+)_{\rm A}$ contribution does not result in a significantly improvement of fit, but the fit fractions of the two amplitudes are much different with the assumption of only $K^-a_1^+(1260)$ and are nearly 100% correlated. We avoid this kind of case and only consider the resonant term, in agreement with the analysis of Mark III [7]. For the process $D^0 \to K_1^-(1270)\pi^+$ with $K_1^-(1270)[S] \to \bar{K}^{*0}\pi^-$, the corresponding significance is found to be 4.3σ only, but we still include it in the fit since the corresponding D-wave process is found to have a statistical significance of larger than 9σ. Better projections in the invariant mass spectra and an improved fit quality χ^2 are also seen with this S-wave process included.

Finally, we retain 23 processes categorized into 7 components. The other processes, not used in our nominal results but have been tested when determining the nominal fit model, are listed in Appendix A. The widths and masses of $\bar{K}^{*0}$ and ρ^0 are determined by the fit. The results of are listed in Table III. The $K_1^-(1270)$ has a small fit fraction, and we fix its mass and width to the PDG values [1]. The $a_1^+(1260)$ has a mass close to the upper boundary of the $\pi^+\pi^+\pi^-$ invariant mass spectrum. Therefore, we determine its mass and width with a likelihood scan, as shown in Fig. 2. The scan results are

TABLE III. Masses and widths of intermediate resonances $\bar{K}^{*0}$ and ρ^0, the first and second uncertainties are statistical and systematic, respectively.

Resonances	Mass (MeV/c^2)	Width (MeV/c^2)
$\bar{K}^{*0}$	$894.78 \pm 0.75 \pm 1.66$	$44.18 \pm 1.57 \pm 1.39$
ρ^0	$779.14 \pm 1.68 \pm 3.98$	$148.42 \pm 2.87 \pm 3.36$

$$\begin{aligned} m_{a_1^+(1260)} &= 1362 \pm 13 \ \ {\rm MeV}/c^2, \\ \Gamma_{a_1^+(1260)} &= 542 \pm 29 \ \ {\rm MeV}/c^2, \end{aligned} \tag{30}$$

where the uncertainties are statistical only. The mass and width of $a_1^+(1260)$ are fixed to the scanned values in the nominal fit.

Our nominal fit yields a goodness of fit value of $\chi^2/\nu = 843.445/748 = 1.128$. To calculate the statistical significance of a process, we repeat the fit process without the corresponding process included, and the changes of log likelihood value and the number of free degree are taking into consideration. All of the components, amplitudes and the significance of amplitudes are listed in Table IV. The fit fractions of all components are given in Table V. The phases and fit fractions of all amplitudes are given in Table VI.

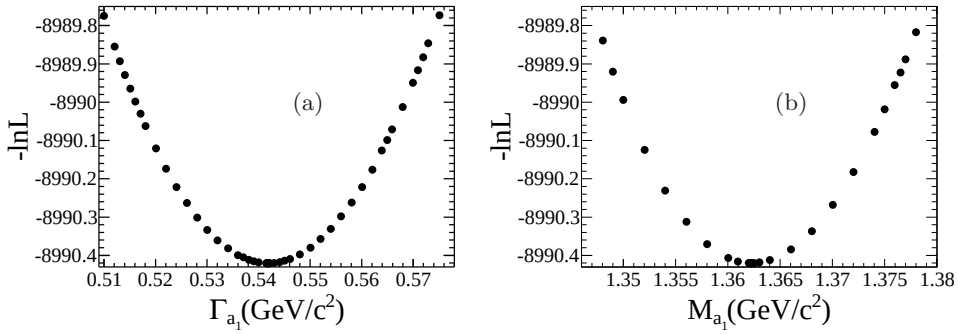

FIG. 2. Likelihood scans of the width (a) and mass (b) of $a_1^+(1260)$.

TABLE IV. Statistical significances for different amplitudes.

Component	Amplitude	significance (σ)
$D^0 \to \bar{K}^{*0}\rho^0$	$D^0[S] \to \bar{K}^{*0}\rho^0$	> 10.0
	$D^0[P] \to \bar{K}^{*0}\rho^0$	> 10.0
	$D^0[D] \to \bar{K}^{*0}\rho^0$	> 10.0
$D^0 \to K^- a_1^+(1260)$, $a_1^+(1260) \to \rho^0\pi^+$	$D^0 \to K^- a_1^+(1260)$, $a_1^+(1260)[S] \to \rho^0\pi^+$	> 10.0
	$D^0 \to K^- a_1^+(1260)$, $a_1^+(1260)[D] \to \rho^0\pi^+$	7.4
$D^0 \to K_1^-(1270)\pi^+$, $K_1^-(1270) \to \bar{K}^{*0}\pi^-$	$D^0 \to K_1^-(1270)\pi^+$, $K_1^-(1270)[S] \to \bar{K}^{*0}\pi^-$	4.3
	$D^0 \to K_1^-(1270)\pi^+$, $K_1^-(1270)[D] \to \bar{K}^{*0}\pi^-$	9.6
$D^0 \to K_1^-(1270)\pi^+$, $K_1^-(1270) \to K^-\rho^0$	$D^0 \to K_1^-(1270)\pi^+$, $K_1^-(1270)[S] \to K^-\rho^0$	> 10.0
$D^0 \to K^-\pi^+\rho^0$	$D^0 \to (\rho^0 K^-)_{\rm A}\pi^+$, $(\rho^0 K^-)_{\rm A}[D] \to K^-\rho^0$	9.6
	$D^0 \to (K^-\rho^0)_{\rm P}\pi^+$	7.0
	$D^0 \to (K^-\pi^+)_{\rm S-wave}\rho^0$	5.1
	$D^0 \to (K^-\rho^0)_{\rm V}\pi^+$	6.8
$D^0 \to \bar{K}^{*0}\pi^+\pi^-$	$D^0 \to (\bar{K}^{*0}\pi^-)_{\rm P}\pi^+$	8.5
	$D^0 \to \bar{K}^{*0}(\pi^+\pi^-)_{\rm S}$	8.9
	$D^0 \to (\bar{K}^{*0}\pi^-)_{\rm V}\pi^+$	9.7
$D \to K^-\pi^+\pi^+\pi^-$	$D^0 \to ((K^-\pi^+)_{\rm S-wave}\pi^-)_{\rm A}\pi^+$	> 10.0
	$D^0 \to K^-((\pi^+\pi^-)_{\rm S}\pi^+)_{\rm A}$	> 10.0
	$D^0 \to (K^-\pi^+)_{\rm S-wave}(\pi^+\pi^-)_{\rm S}$	> 10.0
	$D^0[S] \to (K^-\pi^+)_{\rm V}(\pi^+\pi^-)_{\rm V}$	8.8
	$D^0 \to (K^-\pi^+)_{\rm S-wave}(\pi^+\pi^-)_{\rm V}$	5.8
	$D^0 \to (K^-\pi^+)_{\rm V}(\pi^+\pi^-)_{\rm S}$	> 10.0
	$D^0 \to (K^-\pi^+)_{\rm T}(\pi^+\pi^-)_{\rm S}$	6.8
	$D^0 \to (K^-\pi^+)_{\rm S-wave}(\pi^+\pi^-)_{\rm T}$	9.7

TABLE V. Fit fractions for different components. The first and second uncertainties are statistical and systematic, respectively.

Component	Fit fraction (%)	Mark III's result	E691's result
$D^0 \to \bar{K}^{*0}\rho^0$	$12.3 \pm 0.4 \pm 0.5$	$14.2 \pm 1.6 \pm 5$	$13 \pm 2 \pm 2$
$D^0 \to K^- a_1^+(1260)(\rho^0\pi^+)$	$54.6 \pm 2.8 \pm 3.7$	$49.2 \pm 2.4 \pm 8$	$47 \pm 5 \pm 10$
$D^0 \to K_1^-(1270)(\bar{K}^{*0}\pi^-)\pi^+$	$0.8 \pm 0.2 \pm 0.2$	$6.6 \pm 1.9 \pm 3$	-
$D^0 \to K_1^-(1270)(K^-\rho^0)\pi^+$	$3.4 \pm 0.3 \pm 0.5$		
$D^0 \to K^-\pi^+\rho^0$	$8.4 \pm 1.1 \pm 2.5$	$8.4 \pm 2.2 \pm 4$	$5 \pm 3 \pm 2$
$D^0 \to \bar{K}^{*0}\pi^+\pi^-$	$7.0 \pm 0.4 \pm 0.5$	$14.0 \pm 1.8 \pm 4$	$11 \pm 2 \pm 3$
$D^0 \to K^-\pi^+\pi^+\pi^-$	$21.9 \pm 0.6 \pm 0.6$	$24.2 \pm 2.5 \pm 6$	$23 \pm 2 \pm 3$

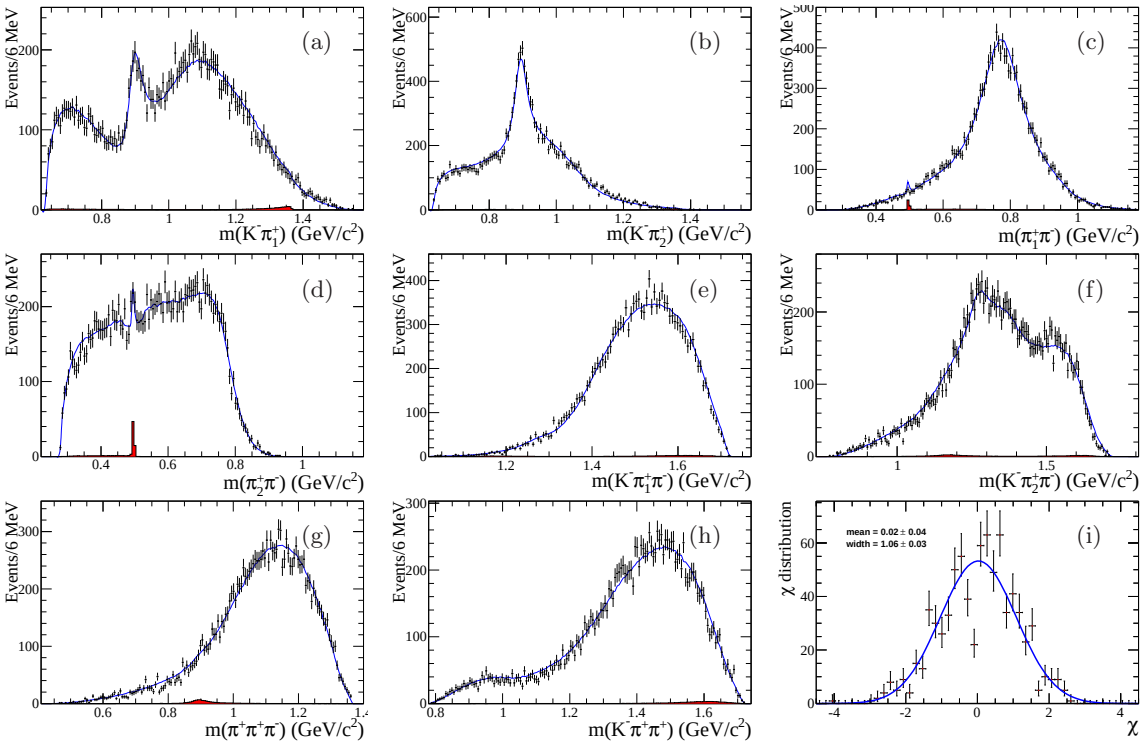

FIG. 3. Distribution of (a) $m_{K^-\pi_1^+}$, (b) $m_{K^-\pi_2^+}$, (c) $m_{\pi_1^+\pi^-}$, (d) $m_{\pi_2^+\pi^-}$, (e) $m_{K^-\pi_1^+\pi^-}$, (f) $m_{K^-\pi_2^+\pi^-}$, (g) $m_{\pi_1^+\pi_2^+\pi^-}$ and (h) $m_{K^-\pi_1^+\pi_2^+}$, where the dots with error are data, and curves are for the fit projections. The small red histograms in each projection shows the $D^0 \to K^0_S K^-\pi^+$ peaking background. In (d), a peak of K^0_S can be seen, which is consistent with the MC expectation. The dip around the K^0_S peak is caused by the requirements used to suppress the $D^0 \to K^0_S K^-\pi^+$ background. Plot (i) shows the fit (curve) to the distribution of the χ (points with error bars) with a Gaussian function and the fitted values of the parameters (mean and width of Gaussian).

TABLE VI. Phases and fit fractions for different amplitudes. The first and second uncertainties are statistical and systematic, respectively.

Amplitude	ϕ_i	Fit fraction (%)
$D^0[S] \to \bar{K}^*\rho^0$	$2.35 \pm 0.06 \pm 0.18$	$6.5 \pm 0.5 \pm 0.8$
$D^0[P] \to \bar{K}^*\rho^0$	$-2.25 \pm 0.08 \pm 0.15$	$2.3 \pm 0.2 \pm 0.1$
$D^0[D] \to \bar{K}^*\rho^0$	$2.49 \pm 0.06 \pm 0.11$	$7.9 \pm 0.4 \pm 0.7$
$D^0 \to K^- a_1^+(1260)$, $a_1^+(1260)[S] \to \rho^0\pi^+$	0(fixed)	$53.2 \pm 2.8 \pm 4.0$
$D^0 \to K^- a_1^+(1260)$, $a_1^+(1260)[D] \to \rho^0\pi^+$	$-2.11 \pm 0.15 \pm 0.21$	$0.3 \pm 0.1 \pm 0.1$
$D^0 \to K_1^-(1270)\pi^+$, $K_1^-(1270)[S] \to \bar{K}^{*0}\pi^-$	$1.48 \pm 0.21 \pm 0.24$	$0.1 \pm 0.1 \pm 0.1$
$D^0 \to K_1^-(1270)\pi^+$, $K_1^-(1270)[D] \to \bar{K}^{*0}\pi^-$	$3.00 \pm 0.09 \pm 0.15$	$0.7 \pm 0.2 \pm 0.2$
$D^0 \to K_1^-(1270)\pi^+$, $K_1^-(1270) \to K^-\rho^0$	$-2.46 \pm 0.06 \pm 0.21$	$3.4 \pm 0.3 \pm 0.5$
$D^0 \to (\rho^0 K^-)_{\rm A}\pi^+$, $(\rho^0 K^-)_{\rm A}[D] \to K^-\rho^0$	$-0.43 \pm 0.09 \pm 0.12$	$1.1 \pm 0.2 \pm 0.3$
$D^0 \to (K^-\rho^0)_{\rm P}\pi^+$	$-0.14 \pm 0.11 \pm 0.10$	$7.4 \pm 1.6 \pm 5.7$
$D^0 \to (K^-\pi^+)_{\rm S-wave}\rho^0$	$-2.45 \pm 0.19 \pm 0.47$	$2.0 \pm 0.7 \pm 1.9$
$D^0 \to (K^-\rho^0)_{\rm V}\pi^+$	$-1.34 \pm 0.12 \pm 0.09$	$0.4 \pm 0.1 \pm 0.1$
$D^0 \to (\bar{K}^{*0}\pi^-)_{\rm P}\pi^+$	$-2.09 \pm 0.12 \pm 0.22$	$2.4 \pm 0.5 \pm 0.5$
$D^0 \to \bar{K}^{*0}(\pi^+\pi^-)_{\rm S}$	$-0.17 \pm 0.11 \pm 0.12$	$2.6 \pm 0.6 \pm 0.6$
$D^0 \to (\bar{K}^{*0}\pi^-)_{\rm V}\pi^+$	$-2.13 \pm 0.10 \pm 0.11$	$0.8 \pm 0.1 \pm 0.1$
$D^0 \to ((K^-\pi^+)_{\rm S-wave}\pi^-)_{\rm A}\pi^+$	$-1.36 \pm 0.08 \pm 0.37$	$5.6 \pm 0.9 \pm 2.7$
$D^0 \to K^-((\pi^+\pi^-)_{\rm S}\pi^+)_{\rm A}$	$-2.23 \pm 0.08 \pm 0.22$	$13.1 \pm 1.9 \pm 2.2$
$D^0 \to (K^-\pi^+)_{\rm S-wave}(\pi^+\pi^-)_{\rm S}$	$-1.40 \pm 0.04 \pm 0.22$	$16.3 \pm 0.5 \pm 0.6$
$D^0[S] \to (K^-\pi^+)_{\rm V}(\pi^+\pi^-)_{\rm V}$	$1.59 \pm 0.13 \pm 0.41$	$5.4 \pm 1.2 \pm 1.9$
$D^0 \to (K^-\pi^+)_{\rm S-wave}(\pi^+\pi^-)_{\rm V}$	$-0.16 \pm 0.17 \pm 0.43$	$1.9 \pm 0.6 \pm 1.2$
$D^0 \to (K^-\pi^+)_{\rm V}(\pi^+\pi^-)_{\rm S}$	$2.58 \pm 0.08 \pm 0.25$	$2.9 \pm 0.5 \pm 1.7$
$D^0 \to (K^-\pi^+)_{\rm T}(\pi^+\pi^-)_{\rm S}$	$-2.92 \pm 0.14 \pm 0.12$	$0.3 \pm 0.1 \pm 0.1$
$D^0 \to (K^-\pi^+)_{\rm S-wave}(\pi^+\pi^-)_{\rm T}$	$2.45 \pm 0.12 \pm 0.37$	$0.5 \pm 0.1 \pm 0.1$

VI. SYSTEMATIC UNCERTAINTIES

The source of systematic uncertainties are divided into four categories: (I) amplitude model, (II) background estimation, (III) experimental effects and (IV) fitter performance. The systematic uncertainties of the free parameters in the fit and the fit fractions due to different contributions are given in units of the statistical standard deviations σ_{stat} in Tables VII–IX. These uncertainties are added in quadrature, as they are uncorrelated, to obtain the total systematic uncertainties.

TABLE VII. Systematic uncertainties on masses and widths of intermediate resonances $\bar{K}^{*0}$ and ρ^0.

Parameter	Source (σ_{stat})				total (σ_{stat})
	I	II	III	IV	
$m_{\bar{K}^{*0}}$	2.21	0.04	0.13	0.10	2.22
$\Gamma_{\bar{K}^{*0}}$	0.87	0.05	0.17	0.07	0.89
m_{ρ^0}	2.37	0.08	0.12	0.08	2.37
Γ_{ρ^0}	1.16	0.04	0.11	0.12	1.17

1. Amplitude Model

Three sources are considered for the systematic uncertainty due to the amplitude model: the masses and widths of the $K_1^-(1270)$ and the $a_1^+(1260)$, the barrier effective radius R and the fixed parameters in the $K\pi$ S-wave model. The uncertainty associated with the mass and width of $K_1^-(1270)$ and the $a_1^+(1260)$ are estimated by varying the corresponding masses and widths with 1σ of errors quoted in PDG [1], respectively. The uncertainty related to the barrier effective radius R is estimated by varying R within $1.5 \sim 4.5\,\mathrm{GeV}^{-1}$ for the intermediate resonances and $3.0 \sim 7.0\,\mathrm{GeV}^{-1}$ for the D^0 in the fit. The uncertainty from the input parameters of the $K\pi$ S-wave model are evaluated by varying the input values within their uncertainties. All the change of the results with respect to the nominal one are taken as the systematic uncertainties.

2. Background Estimation

The sources of systematic uncertainty related to the background include the amplitude and shape of the background $D^0 \to K^0_S K^-\pi^+$, and the other potential backgrounds. The uncertainties related to the background $D^0 \to K^0_S K^-\pi^+$ is estimated by varying the number of background events within 1σ of uncertainties and changing the shape according to the uncertainties in PDF parameters from CLEO [18]. The uncertainty due to the the other potential background is estimated by including the corresponding background (estimated from generic MC sample) in the fit.

3. Experimental Effects

The uncertainty related to the experimental effects includes two separate components: the acceptance difference between MC and data caused by tracking and PID efficiencies, and the detector resolution. To determine the systematic uncertainty due to tracking and PID efficiencies, we alter the fit by shifting the $\gamma_\epsilon(p)$ in Eq. (9) within its uncertainty, and the changes of the nominal results is taken as the systematic uncertainty. The uncertainty caused by resolution is determined as the difference between the pull distribution results obtained from simulated data using generated and fitted four-momenta, as described in Sec. VI 4.

4. Fitter Performance

The uncertainty from the fit process is evaluated by studying toy MC samples. An ensemble of 250 sets of SIGNAL MC samples with a size equal to the data sample are generated according to the nominal results in this analysis. The SIGNAL MC samples are fed into the event selection, and the same amplitude analysis is performed on each simulated sample. The pull variables, $\frac{V_{\rm input}-V_{\rm fit}}{\sigma_{\rm fit}}$, are defined to evaluate the corresponding uncertainty, where $V_{\rm input}$ is the input value in the generator, $V_{\rm fit}$ and $\sigma_{\rm fit}$ are the output value and the corresponding statistical uncertainty, respectively. The distribution of pull values for the 250 sets of sample are expected to be a normal Gaussian distribution, and any shift on mean and widths indicate the bias on the fit values and its statistical uncertainty, respectively.

Small biases for some fitted parameters and fit fractions are observed. For the pull mean, the largest bias is about 19% of a statistical uncertainty with a deviation of about 3.0σ from zero. For the pull width, the largest shift is 0.87 ± 0.04, about 3.0 standard deviations from 1.0. We add in quadrature the mean and the mean error in the pull and multiply this number with the statistical error to get the systematic error. The fit results are given in Tables X–XII. The uncertainties in Tables X–XII are the statistical uncertainties of the fits to the pull distributions.

TABLE VIII. Systematic uncertainties on fit fractions for different components.

Fit fraction	Source (σ_{stat}) I	II	III	IV	total (σ_{stat})
$D^0 \to K^{*0}\rho^0$	1.12	0.06	0.11	0.08	1.13
$D^0 \to K^- a_1^+(1260)$	1.32	0.09	0.12	0.06	1.33
$D^0 \to K_1^-(1270)(\bar{K}^{*0}\pi^-)\pi^+$	1.41	0.02	0.12	0.10	1.42
$D^0 \to K_1^-(1270)(K^-\rho^0)\pi^+$	1.58	0.04	0.23	0.06	1.60
$D^0 \to K^-\pi^+\rho^0$	2.22	0.10	0.12	0.15	2.23
$D^0 \to \bar{K}^{*0}\pi^+\pi^-$	1.32	0.08	0.13	0.10	1.34
$D^0 \to K^-\pi^+\pi^+\pi^-$	0.94	0.10	0.09	0.12	1.00

TABLE IX. Systematic uncertainties on phases and fit fractions for different amplitudes.

ϕ_i	Source (σ_{stat}) I	II	III	IV	total (σ_{stat})
$D^0[S] \to K^{*0}\rho^0$	2.96	0.04	0.14	0.13	2.97
$D^0[P] \to \bar{K}^{*0}\rho^0$	1.98	0.04	0.11	0.12	1.98
$D^0[D] \to \bar{K}^{*0}\rho^0$	1.78	0.03	0.18	0.09	1.79
$D^0 \to K^- a_1^+(1260)$, $a_1^+(1260)[D] \to \rho^0\pi^+$	1.38	0.02	0.09	0.09	1.39
$D^0 \to K_1^-(1270)\pi^+$,$K_1^-(1270)[S] \to \bar{K}^{*0}\pi^-$	1.10	0.07	0.10	0.09	1.11
$D^0 \to K_1^-(1270)\pi^+$,$K_1^-(1270)[D] \to \bar{K}^{*0}\pi^-$	1.61	0.06	0.11	0.06	1.62
$D^0 \to K_1^-(1270)\pi^+$,$K_1^-(1270) \to K^-\rho^0$	3.61	0.03	0.09	0.13	3.62
$D^0 \to (\rho^0 K^-)_{\rm A}\pi^+$	1.28	0.06	0.14	0.09	1.29
$D^0 \to (K^-\rho^0)_{\rm P}\pi^+$	0.92	0.10	0.10	0.07	0.93
$D^0 \to (K^-\pi^+)_{\rm S-wave}\rho^0$	2.46	0.06	0.10	0.09	2.47
$D^0 \to (K^-\rho^0)_{\rm V}\pi^+$	0.74	0.01	0.09	0.08	0.75
$D^0 \to (\bar{K}^{*0}\pi^-)_{\rm P}\pi^+$	1.82	0.03	0.09	0.06	1.82
$D^0 \to \bar{K}^*(\pi^+\pi^-)_{\rm S}$	1.07	0.04	0.12	0.11	1.08
$D^0 \to (\bar{K}^{*0}\pi^-)_{\rm V}\pi^+$	1.00	0.02	0.10	0.18	1.02
$D^0 \to ((K^-\pi^+)_{\rm S-wave}\pi^-)_{\rm A}\pi^+$	4.78	0.15	0.12	0.07	4.79
$D^0 \to K^-((\pi^+\pi^-)_{\rm S}\pi^+)_{\rm A}$	2.69	0.13	0.10	0.07	2.70
$D^0 \to (K^-\pi^+)_{\rm S-wave}(\pi^+\pi^-)_{\rm S}$	6.27	0.04	0.10	0.12	6.27
$D^0[S] \to (K^-\pi^+)_{\rm V}(\pi^+\pi^-)_{\rm V}$	3.28	0.06	0.09	0.06	3.28
$D^0 \to (K^-\pi^+)_{\rm S-wave}(\pi^+\pi^-)_{\rm V}$	2.59	0.09	0.10	0.10	2.60
$D^0 \to (K^-\pi^+)_{\rm V}(\pi^+\pi^-)_{\rm S}$	3.07	0.09	0.10	0.18	3.08
$D^0 \to (K^-\pi^+)_{\rm T}(\pi^+\pi^-)_{\rm S}$	0.81	0.04	0.12	0.06	0.82
$D^0 \to (K^-\pi^+)_{\rm S-wave}(\pi^+\pi^-)_{\rm T}$	3.11	0.06	0.11	0.16	3.19
Fit fraction	Source (σ_{stat}) I	II	III	IV	total (σ_{stat})
$D^0[S] \to K^{*0}\rho^0$	1.76	0.04	0.09	0.10	1.77
$D^0[P] \to \bar{K}^{*0}\rho^0$	0.27	0.02	0.09	0.12	0.31
$D^0[D] \to \bar{K}^{*0}\rho^0$	1.79	0.06	0.12	0.17	1.80
$D^0 \to K^- a_1^+(1260)$, $a_1^+(1260)[S] \to \rho^0\pi^+$	1.48	0.10	0.12	0.07	1.45
$D^0 \to K^- a_1^+(1260)$, $a_1^+(1260)[D] \to \rho^0\pi^+$	0.93	0.04	0.09	0.06	0.94
$D^0 \to K_1^-(1270)\pi^+$,$K_1^-(1270)[S] \to \bar{K}^{*0}\pi^-$	1.01	0.05	0.11	0.16	1.03
$D^0 \to K_1^-(1270)\pi^+$,$K_1^-(1270)[D] \to \bar{K}^{*0}\pi^-$	1.12	0.03	0.12	0.13	1.14
$D^0 \to K_1(1270)^-\pi^+$,$K_1^-(1270) \to K^-\rho^0$	1.58	0.04	0.23	0.06	1.60
$D^0 \to (\rho^0 K^-)_{\rm A}\pi^+$	1.38	0.08	0.09	0.09	1.39
$D^0 \to (\bar{K}^{*0}\pi)_{\rm P}\pi$	0.93	0.06	0.09	0.16	0.95
$D^0 \to (K^-\pi^+)_{\rm S-wave}\rho^0$	2.81	0.09	0.11	0.09	2.82
$D^0 \to (K^-\rho^0)_{\rm V}\pi^+$	0.69	0.03	0.09	0.06	0.70
$D^0 \to (\bar{K}^{*0}\pi^-)_{\rm P}\pi^+$	0.93	0.06	0.09	0.16	0.95
$D^0 \to \bar{K}^{*0}(\pi^+\pi^-)_{\rm S}$	1.06	0.05	0.09	0.20	1.08
$D^0 \to (\bar{K}^{*0}\pi^-)_{\rm V}\pi^+$	0.60	0.02	0.00	0.10	0.61
$D^0 \to ((K^-\pi^+)_{\rm S-wave}\pi^-)_{\rm A}\pi^+$	3.10	0.07	0.09	0.06	3.10
$D^0 \to K^-((\pi^+\pi^-)_{\rm S}\pi^+)_{\rm A}$	1.14	0.08	0.10	0.07	1.15
$D^0 \to (K^-\pi^+)_{\rm S-wave}(\pi^+\pi^-)_{\rm S}$	1.29	0.12	0.10	0.12	1.30
$D^0[S] \to (K^-\pi^+)_{\rm V}(\pi^+\pi^-)_{\rm V}$	1.73	0.07	0.09	0.07	1.73
$D^0 \to (K^-\pi^+)_{\rm S-wave}(\pi^+\pi^-)_{\rm V}$	2.08	0.12	0.10	0.07	2.09
$D^0 \to (K^-\pi^+)_{\rm V}(\pi^+\pi^-)_{\rm S}$	3.54	0.05	0.10	0.11	3.54
$D^0 \to (K^-\pi^+)_{\rm T}(\pi^+\pi^-)_{\rm S}$	0.87	0.07	0.11	0.07	0.88
$D^0 \to (K^-\pi^+)_{\rm S-wave}(\pi^+\pi^-)_{\rm T}$	0.99	0.09	0.10	0.08	1.01

TABLE X. Pull mean and pull width of the pull distributions for the fitted masses and widths of intermediate resonances $\bar{K}^{*0}$ and ρ^0 from simulated data using either the generated or fitted four-momenta.

Parameter	Generated p_i		Fitted p_i	
	pull mean	pull width	pull mean	pull width
$m_{\bar{K}^{*0}}$	0.07 ± 0.07	1.05 ± 0.05	0.06 ± 0.07	1.04 ± 0.05
$\Gamma_{\bar{K}^{*0}}$	-0.03 ± 0.06	0.97 ± 0.04	-0.17 ± 0.06	0.97 ± 0.04
m_{ρ^0}	0.03 ± 0.07	1.06 ± 0.05	-0.02 ± 0.07	1.06 ± 0.05
Γ_{ρ^0}	0.10 ± 0.07	1.08 ± 0.05	0.06 ± 0.07	1.07 ± 0.05

TABLE XI. Pull mean and pull width of the pull distributions for the different components from simulated data using either the generated or fitted four-momenta.

Fit fraction	Generated p_i		Fitted p_i	
	pull mean	pull width	pull mean	pull width
$D^0 \to K^{*0}\rho^0$	0.05 ± 0.06	0.92 ± 0.04	0.04 ± 0.06	0.89 ± 0.04
$D^0 \to K^- a_1^+(1260)$	0.02 ± 0.06	0.91 ± 0.04	0.04 ± 0.06	0.87 ± 0.04
$D^0 \to K_1^-(1270)(\bar{K}^{*0}\pi^-)\pi^+$	-0.08 ± 0.06	0.98 ± 0.04	-0.06 ± 0.06	0.97 ± 0.04
$D^0 \to K_1^-(1270)(K^-\rho^0)\pi^+$	0.01 ± 0.06	0.98 ± 0.04	0.01 ± 0.06	0.99 ± 0.04
$D^0 \to K^-\pi^+\rho^0$	0.14 ± 0.06	0.92 ± 0.04	0.11 ± 0.06	0.88 ± 0.04
$D^0 \to \bar{K}^{*0}\pi^+\pi^-$	-0.08 ± 0.06	0.96 ± 0.04	-0.09 ± 0.06	0.96 ± 0.04
$D^0 \to K^-\pi^+\pi^+\pi^-$	0.10 ± 0.06	0.94 ± 0.04	0.12 ± 0.06	0.93 ± 0.04

TABLE XII. Pull mean and pull width of the pull distributions for the phases and fit fractions of different amplitudes, from simulated data using either the generated or fitted four-momenta.

ϕ_i	Generated p_i		Fitted p_i	
	pull mean	pull width	pull mean	pull width
$D^0[S] \to K^{*0}\rho^0$	0.11 ± 0.06	1.01 ± 0.05	0.08 ± 0.06	1.00 ± 0.04
$D^0[P] \to \bar{K}^{*0}\rho^0$	0.10 ± 0.07	1.03 ± 0.05	0.08 ± 0.06	1.02 ± 0.05
$D^0[D] \to \bar{K}^{*0}\rho^0$	0.05 ± 0.07	1.04 ± 0.05	0.01 ± 0.07	1.03 ± 0.05
$D^0 \to K^- a_1^+(1260)$, $a_1^+(1260)[D] \to \rho^0\pi^+$	-0.07 ± 0.06	1.02 ± 0.05	-0.05 ± 0.06	1.02 ± 0.05
$D^0 \to K_1^-(1270)\pi^+$,$K_1^-(1270)[S] \to \bar{K}^{*0}\pi^-$	0.06 ± 0.07	1.03 ± 0.05	0.06 ± 0.06	1.03 ± 0.05
$D^0 \to K_1^-(1270)\pi^+$,$K_1^-(1270)[D] \to \bar{K}^{*0}\pi^-$	-0.02 ± 0.06	0.98 ± 0.04	-0.06 ± 0.06	0.97 ± 0.04
$D^0 \to K_1^-(1270)\pi^+$,$K_1^-(1270) \to K^-\rho^0$	0.12 ± 0.06	1.00 ± 0.04	0.11 ± 0.06	1.00 ± 0.04
$D^0 \to (\rho^0 K^-)_{\rm A}\pi^+$	-0.06 ± 0.07	1.05 ± 0.05	-0.09 ± 0.07	1.05 ± 0.05
$D^0 \to (K^-\rho^0)_{\rm P}\pi^+$	-0.03 ± 0.06	0.96 ± 0.04	-0.01 ± 0.06	0.96 ± 0.04
$D^0 \to (K^-\pi^+)_{\rm S-wave}\rho^0$	-0.07 ± 0.06	0.92 ± 0.04	-0.08 ± 0.06	0.92 ± 0.04
$D^0 \to (K^-\rho^0)_{\rm V}\pi^+$	-0.05 ± 0.06	1.02 ± 0.05	-0.07 ± 0.06	1.01 ± 0.05
$D^0 \to (\bar{K}^{*0}\pi^-)_{\rm P}\pi^+$	0.00 ± 0.06	0.99 ± 0.04	0.00 ± 0.06	0.99 ± 0.04
$D^0 \to \bar{K}^{*0}(\pi^+\pi^-)_{\rm S}$	-0.08 ± 0.07	1.03 ± 0.05	-0.11 ± 0.07	1.03 ± 0.05
$D^0 \to (\bar{K}^{*0}\pi^-)_{\rm V}\pi^+$	0.17 ± 0.06	0.99 ± 0.04	0.15 ± 0.06	0.98 ± 0.04
$D^0 \to ((K^-\pi^+)_{\rm S-wave}\pi^-)_{\rm A}\pi^+$	-0.04 ± 0.06	0.92 ± 0.04	0.02 ± 0.06	0.92 ± 0.04
$D^0 \to K^-((\pi^+\pi^-)_{\rm S}\pi^+)_{\rm A}$	0.00 ± 0.07	1.05 ± 0.05	-0.02 ± 0.07	1.04 ± 0.05
$D^0 \to (K^-\pi^+)_{\rm S-wave}(\pi^+\pi^-)_{\rm S}$	0.10 ± 0.06	0.98 ± 0.04	0.08 ± 0.06	0.98 ± 0.04
$D^0[S] \to (K^-\pi^+)_{\rm V}(\pi^+\pi^-)_{\rm V}$	-0.02 ± 0.06	0.97 ± 0.04	-0.03 ± 0.06	0.98 ± 0.04
$D^0 \to (K^-\pi^+)_{\rm S-wave}(\pi^+\pi^-)_{\rm V}$	0.08 ± 0.06	0.93 ± 0.04	0.06 ± 0.06	0.92 ± 0.04
$D^0 \to (K^-\pi^+)_{\rm V}(\pi^+\pi^-)_{\rm S}$	-0.17 ± 0.06	0.94 ± 0.04	-0.17 ± 0.06	0.94 ± 0.04
$D^0 \to (K^-\pi^+)_{\rm T}(\pi^+\pi^-)_{\rm S}$	0.01 ± 0.06	1.01 ± 0.05	-0.02 ± 0.06	1.00 ± 0.04
$D^0 \to (K^-\pi^+)_{\rm S-wave}(\pi^+\pi^-)_{\rm T}$	0.14 ± 0.07	1.12 ± 0.05	0.12 ± 0.07	1.11 ± 0.05
Fit fraction	Generated p_i		Fitted p_i	
	pull mean	pull width	pull mean	pull width
$D^0[S] \to K^{*0}\rho^0$	0.08 ± 0.06	0.88 ± 0.04	0.07 ± 0.06	0.87 ± 0.04
$D^0[P] \to \bar{K}^{*0}\rho^0$	0.10 ± 0.06	0.97 ± 0.04	0.10 ± 0.06	0.96 ± 0.04
$D^0[D] \to \bar{K}^{*0}\rho^0$	-0.15 ± 0.07	1.10 ± 0.05	-0.15 ± 0.07	1.10 ± 0.05
$D^0 \to K^- a_1^+(1260)$, $a_1^+(1260)[S] \to \rho^0\pi^+$	0.03 ± 0.06	0.91 ± 0.04	0.04 ± 0.06	0.90 ± 0.04
$D^0 \to K^- a_1^+(1260)$, $a_1^+(1260)[D] \to \rho^0\pi^+$	0.02 ± 0.06	1.00 ± 0.04	0.03 ± 0.06	1.00 ± 0.04
$D^0 \to K_1^-(1270)\pi$,$K_1^-(1270)[S] \to \bar{K}^{*0}\pi^-$	-0.14 ± 0.07	1.02 ± 0.05	-0.18 ± 0.07	1.09 ± 0.05
$D \to K_1^-(1270)\pi^+$,$K_1^-(1270)[D] \to \bar{K}^{*0}\pi^-$	-0.11 ± 0.06	0.99 ± 0.04	-0.09 ± 0.06	0.99 ± 0.04
$D^0 \to K_1^-(1270)\pi^+$,$K_1^-(1270) \to K^-\rho^0$	0.01 ± 0.06	0.98 ± 0.04	0.01 ± 0.06	0.98 ± 0.04
$D^0 \to (\rho^0 K^-)_{\rm A}\pi^+$	0.06 ± 0.06	1.00 ± 0.04	0.04 ± 0.06	0.99 ± 0.04
$D^0 \to (K^-\rho^0)_{\rm P}\pi^+$	0.11 ± 0.06	0.95 ± 0.04	0.09 ± 0.06	0.94 ± 0.04
$D^0 \to (K^-\pi^+)_{\rm S-wave}\rho^0$	0.05 ± 0.07	1.04 ± 0.05	0.05 ± 0.07	1.04 ± 0.05
$D^0 \to (K^-\rho^0)_{\rm V}\pi^+$	0.01 ± 0.06	0.98 ± 0.04	0.02 ± 0.06	0.97 ± 0.04
$D^0 \to (\bar{K}^{*0}\pi^-)_{\rm P}\pi^+$	0.15 ± 0.06	0.93 ± 0.04	0.15 ± 0.06	0.93 ± 0.04
$D^0 \to \bar{K}^{*0}(\pi^+\pi^-)_{\rm S}$	-0.19 ± 0.06	1.03 ± 0.05	-0.18 ± 0.06	1.02 ± 0.05
$D^0 \to (\bar{K}^{*0}\pi^-)_{\rm V}\pi^+$	-0.08 ± 0.06	1.00 ± 0.04	-0.09 ± 0.06	1.00 ± 0.04
$D^0 \to ((K^-\pi^+)_{\rm S-wave}\pi^-)_{\rm A}\pi^+$	0.02 ± 0.06	0.98 ± 0.04	0.02 ± 0.06	0.97 ± 0.04
$D^0 \to K^-((\pi^+\pi^-)_{\rm S}\pi^+)_{\rm A}$	0.04 ± 0.06	1.01 ± 0.05	0.04 ± 0.06	1.00 ± 0.04
$D^0 \to (K^-\pi^+)_{\rm S-wave}(\pi^+\pi^-)_{\rm S}$	-0.10 ± 0.06	0.93 ± 0.04	-0.09 ± 0.06	0.93 ± 0.04
$D^0[S] \to (K^-\pi^+)_{\rm V}(\pi^+\pi^-)_{\rm V}$	0.03 ± 0.06	1.02 ± 0.05	0.03 ± 0.06	1.01 ± 0.05
$D^0 \to (K^-\pi^+)_{\rm S-wave}(\pi^+\pi^-)_{\rm V}$	0.04 ± 0.06	1.00 ± 0.04	0.04 ± 0.06	0.99 ± 0.04
$D^0 \to (K^-\pi^+)_{\rm V}(\pi^+\pi^-)_{\rm S}$	0.09 ± 0.07	1.06 ± 0.05	0.11 ± 0.07	1.04 ± 0.05
$D^0 \to (K^-\pi^+)_{\rm T}(\pi^+\pi^-)_{\rm S}$	0.01 ± 0.07	1.05 ± 0.05	0.00 ± 0.07	1.03 ± 0.05
$D^0 \to (K^-\pi^+)_{\rm S-wave}(\pi^+\pi^-)_{\rm T}$	0.05 ± 0.06	0.96 ± 0.04	0.05 ± 0.06	0.96 ± 0.04

VII. CONCLUSION

An amplitude analysis of the decay $D^0 \to K^-\pi^+\pi^+\pi^-$ has been performed with the 2.93 fb^{-1} of e^+e^- collision data at the $\psi(3770)$ resonance collected by the BESIII detector. The dominant components, $D^0 \to K^- a_1^+(1260)$, $D^0 \to \bar{K}^{*0}\rho^0$, $D^0 \to$ four-body non-resonant decay and three-body non-resonant $D^0 \to K^-\pi^+\rho^0$ improve upon the earlier results from Mark III and are consistent with them within corresponding uncertainties. The resonance $K_1^-(1270)$ observed by Mark III is also confirmed in this analysis. The detailed results are listed in Table V.

About 40% of components comes from the non-resonant four-body ($D^0 \to K^-\pi^+\pi^+\pi^-$) and three-body ($D^0 \to K^-\pi^+\rho^0$ and $D^0 \to \bar{K}^{*0}\pi^+\pi^-$) decays. A detailed study considering the different orbital angular momentum is performed, which was not included in the analyses of Mark III and E691. An especially interesting process involving the $K\pi$ S-wave is described by an effective range parameterization.

By using the inclusive branching fraction $\mathcal{B}(D^0 \to K^-\pi^+\pi^+\pi^-) = (8.07 \pm 0.23)\%$ taken from the PDG [1] and the fit fraction for the different components $FF(n)$ obtained in this analysis, we calculate the exclusive absolute branching fractions for the individual components with $\mathcal{B}(n) = \mathcal{B}(D^0 \to K^-\pi^+\pi^+\pi^-) \times FF(n)$. The results are summarized in Table XIII and are compared with the values quoted in PDG. Our results have much improved precision; They may shed light in theoretical calculation. The knowledge of $D^0 \to \bar{K}^{*0}\rho^0$ and $D^0 \to K^- a_1^+(1260)$ increase our understanding of the decay $D^0 \to VV$ and $D \to AP$, both of which are lacking in experimental measurements, but have large contributions to the D^0 decays. Furthermore, the knowledge of sub-modes in the decay $D^0 \to K^-\pi^+\pi^+\pi^-$ will improve the determination of the reconstruction efficiency when this mode is used to tag D^0 as part of other measurements, like measurements of branching fractions, the strong phase or the angle γ.

TABLE XIII. Absolute branching fractions of the seven components and the corresponding values in the PDG. Here, we denote $\bar{K}^{*0} \to K^-\pi^+$ and $\rho^0 \to \pi^+\pi^-$. The first two uncertainties are statistical and systematic, respectively. The third uncertainties are propagated from the uncertainty of $\mathcal{B}(D^0 \to K^-\pi^+\pi^+\pi^-)$.

Component	Branching fraction (%)	PDG value (%)
$D^0 \to \bar{K}^{*0}\rho^0$	$0.99 \pm 0.04 \pm 0.04 \pm 0.03$	1.05 ± 0.23
$D^0 \to K^- a_1^+(1260)(\rho^0\pi^+)$	$4.41 \pm 0.22 \pm 0.30 \pm 0.13$	3.6 ± 0.6
$D^0 \to K_1^-(1270)(\bar{K}^{*0}\pi^-)\pi^+$	$0.07 \pm 0.01 \pm 0.02 \pm 0.00$	0.29 ± 0.03
$D^0 \to K_1^-(1270)(K^-\rho^0)\pi^+$	$0.27 \pm 0.02 \pm 0.04 \pm 0.01$	
$D^0 \to K^-\pi^+\rho^0$	$0.68 \pm 0.09 \pm 0.20 \pm 0.02$	0.51 ± 0.23
$D^0 \to \bar{K}^{*0}\pi^+\pi^-$	$0.57 \pm 0.03 \pm 0.04 \pm 0.02$	0.99 ± 0.23
$D^0 \to K^-\pi^+\pi^+\pi^-$	$1.77 \pm 0.05 \pm 0.04 \pm 0.05$	1.88 ± 0.26

ACKNOWLEDGMENTS

The BESIII collaboration thanks the staff of BEPCII and the IHEP computing center for their strong support. This work is supported in part by National Key Basic Research Program of China under Contract No. 2015CB856700; National Natural Science Foundation of China (NSFC) under Contracts Nos. 11075174, 11121092, 11125525, 11235011, 11322544, 11335008, 11375221, 11425524, 11475185, 11635010; the Chinese Academy of Sciences (CAS) Large-Scale Scientific Facility Program; Joint Large-Scale Scientific Facility Funds of the NSFC and CAS under Contracts Nos. 11179007, U1232201, U1332201; CAS under Contracts Nos. KJCX2-YW-N29, KJCX2-YW-N45; 100 Talents Program of CAS; INPAC and Shanghai Key Laboratory for Particle Physics and Cosmology; German Research Foundation DFG under Contract No. Collaborative Research Center CRC-1044; Istituto Nazionale di Fisica Nucleare, Italy; Ministry of Development of Turkey under Contract No. DPT2006K-120470; Russian Foundation for Basic Research under Contract No. 14-07-91152; U. S. Department of Energy under Contracts Nos. DE-FG02-04ER41291, DE-FG02-05ER41374, DE-FG02-94ER40823, DESC0010118; U.S. National Science Foundation; University of Groningen (RuG) and the Helmholtzzentrum fuer Schwerionenforschung GmbH (GSI), Darmstadt; WCU Program of National Research Foundation of Korea under Contract No. R32-2008-000-10155-0.

VIII. APPENDIX A: AMPLITUDES TESTED

The amplitudes listed below are tested when determining the nominal fit model, but not used in our final fit result.

- **Cascade amplitudes**
  - $K_1^-(1270)(\rho^0 K^-)\pi^+$, $\rho^0 K^-$ D-wave
  - $K_1^-(1400)(\bar{K}^{*0}\pi^-)\pi^+$, $\bar{K}^{*0}\pi^-$ S and D-waves
  - $K^{*-}(1410)(\bar{K}^{*0}\pi^-)\pi^+$
  - $K_2^{*-}(1430)(\bar{K}^{*0}\pi^-)\pi^+$, $K_2^{*-}(1430)(K^-\rho^0)\pi^+$
  - $K^{*-}(1680)(\bar{K}^{*0}\pi^-)\pi^+$, $K^{*-}(1680)(K^-\rho^0)\pi^+$
  - $K_2^{*-}(1770)(\bar{K}^{*0}\pi^-)\pi^+$, $K_2^{*-}(1770)(K^-\rho^0)\pi^+$
  - $K^- a_2^+(1320)(\rho^0\pi^+)$
  - $K^-\pi^+(1300)(\rho^0\pi^+)$
  - $K^- a_1^+(1260)(f_0(500)\pi^+)$
- **Quasi-two-body amplitudes**
  - $\bar{K}^{*0} f_0(500)$
  - $\bar{K}^{*0} f_0(980)$
- **Three-body amplitudes**

- $\bar{K}^{*0}(\pi^+\pi^-)_{\rm V}$ S, P- and D-waves
- $(K^-\pi^+)_{\rm V}\rho^0$ S, P and D-waves
- $\bar{K}_2^{*0}(1430)(\pi^+\pi^-)_{\rm S}$
- $\bar{K}_2^{*0}(1430)\rho^0$
- $\bar{K}^{*0}f_2(1270)$
- $(K^-\pi^+)_{\rm S}f_2(1270)$
- $K^-(\rho^0\pi^+)_{\rm V}$
- $K^-(\rho^0\pi^+)_{\rm P}$
- $K^-(\rho^0\pi^+)_{\rm A}$
- $K^-(\rho^0\pi^+)_{\rm T}$
- $(\bar{K}^{*0}\pi^-)_{\rm T}\pi^+$
- $(K^-\rho^0)_{\rm T}\pi^+$
- $(\bar{K}^{*0}\pi^-)_{\rm A}\pi^+$, $\bar{K}^{*0}\pi^-$ S and D-waves

- **Four-body non-resonance amplitudes**
  - $(K^-\pi^+)_{\rm T}(\pi^+\pi^-)_{\rm V}$ P- and D-waves
  - $(K^-\pi^+)_{\rm V}(\pi^+\pi^-)_{\rm T}$ P- and D-waves
  - $(K^-\pi^+)_{\rm V}(\pi^+\pi^-)_{\rm V}$ P- and D-waves
  - $(K^-(\pi^+\pi^-)_{\rm S})_{\rm A}\pi^+$

[1] C. Patrignani *et al.* (Particle Data Group), Chin. Phys. C **40**, 100001 (2016).
[2] G. Bonvicini *et al.* (CLEO Collaboration), Phys. Rev. D **89**, 072002 (2014).
[3] D. Atwood, I. Dunietz and A. Soni, Phys. Rev. Lett. **78**, 3257 (1997).
[4] S. Harnew and J. Rademacker, JHEP **03** (2015) 169.
[5] A. F. Falk, Y. Grossman, Z. Ligeti and A. A. Petrov, Phys. Rev. D **65**, 054034 (2002).
[6] H. Y. Cheng and C. W. Chiang, Phys. Rev. D **81**, 114020 (2010).
[7] D. Coffman et al. (Mark III Collaboration), Phys. Rev. D **45**, 2196 (1992).
[8] J. C. Anjos *et al.* (E691 Collaboration), Phys. Rev. D **46**, 1941 (1992).
[9] M. Ablikim *et al.* (BESIII Collaboration), Chin. Phys. C **37**, 123001 (2013).
[10] M. Ablikim *et al.* (BESIII Collaboration), Phys. Lett. B **753**, 629 (2016).
[11] B. S. Zou and D. V. Bugg, Eur. Phys. J. A **16**, 537 (2003).
[12] M. Ablikim *et al.* (BESIII Collaboration), Nucl. Instrum. Methods Phys. Res., Sect. A **614**, 345 (2010).
[13] S. Agostinelli *et al.* (GEANT4 Collaboration), Nucl. Instrum. Methods Phys. Res., Sect. A **506**, 250 (2003).
[14] S. Jadach, B. F. L. Ward and Z. Was, Phys. Rev. D **63**, 113009 (2001).
[15] E. Barberio and Z. was, Comput. Phys. Commun. **79**, 291 (1994).
[16] D. J. Lange, Nucl. Instrum. Methods Phys. Res., Sect. A **462**, 152 (2001);
R. G. Ping, Chin. Phys. C **32**, 599 (2008).
[17] J. C. Chen *et al.*, Phys. Rev. D **62**, 034003 (2000).
[18] J. Insler *et al.* (CLEO Collaboration), Phys. Rev. D **85**, 092016 (2012).
[19] S. U. Chung, Phys. Rev. D **48**, 1225 (1993); **57**, 431 (1998);
F. von Hippel, C. Quigg, Phys. Rev. D **5**, 624 (1972).
[20] G. J. Gounaris, J. J. Sakurai, Phys. Rev. Lett. **21**, 244 (1968).
[21] B. Aubert *et al.* (BABAR Collaboration), Phys. Rev. D **78**, 034023 (2008).
[22] D. Aston *et al.* (LASS Collaboration), Nucl. Phys. B **296**, 493 (1998).